Bioinorganic Molecular Mechanics

Marc Zimmer

Department of Chemistry, Connecticut College, New London, Connecticut 06320

Received March 30, 1995 (Revised Manuscript Received July 7, 1995)

Contents

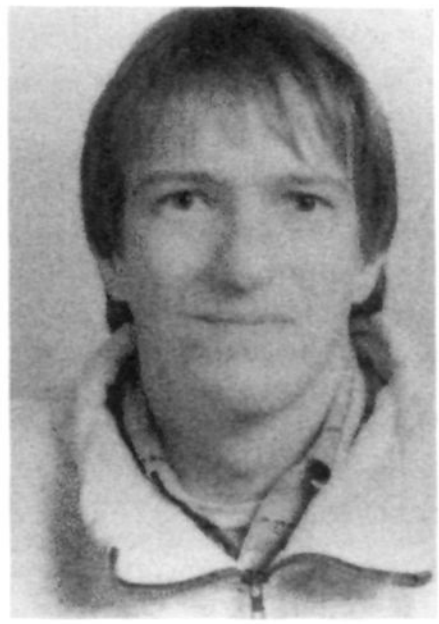

Marc Zimmer was born in Sasolburg, South Africa, in 1961. He received his Bachelor's and Master's degrees from the University of Witwatersrand, where he did his first molecular mechanics calculations under the supervision of Robert Hancock. In 1986 he emigrated to the United States. He worked with Nicholas Kildahl and obtained his Ph.D. in macrocyclic chemistry from the Worcester Polytechnic Institute in 1988. An eighteen-month postdoctoral fellowship with Robert Crabtree at Yale University was responsible for his interest in bioinorganic chemistry. Since 1990, he has been on the faculty of Connecticut College, New London. He has just returned from a sabbatical with Peter Comba in picturesque Heidelberg, Germany. Marc's research interests are (i) the use of cluster analysis in bioinorganic chemistry, (ii) the rational design of bioinorganic complexes using the Cambridge Database, molecular mechanics, and molecular dynamics, and (iii) the molecular mechanical analysis of bleomycin and patellamide complexes.

I. Introduction

The field of transition metal bioinorganic molecular mechanics (MM) is a young and fast developing discipline. This review will attempt to discuss the work published before 1995; it is divided into two main sections. Sections I–IV are an overview of the methods that are used in bioinorganic transition metal MM and section V summarizes the bioinorganic MM literature.

The idea of using a mathematical model, based on the ball and spring concept, to describe the geometry of molecules has been in the literature for more than 50 years.[1–3] Organic force fields such as Allinger's MM1,[4] MM2,[5] and MM3[6] have been used extensively in modeling organic systems. However, bioinorganic MM calculations are limited by a number of factors.

(1) There are no MM programs with reliable bioinorganic force fields.

(2) Organic force fields need to contain parameters for relatively few atoms (C, H, N, O, S). A general bioinorganic force field would have to contain parameters for a number of different transition metals in all their oxidation and spin states, in addition to the organic parameters.

(3) It is difficult to parameterize a bioinorganic MM force field from solid-state structures as there are often insufficient high-resolution crystal structures of analogous molecules.

(4) Deriving force constants from infrared spectra is a not trivial procedure, because metal–ligand vibrational frequencies are low and their analysis is often complicated by strong electronic effects, as well as by mixing with ligand vibrational modes.[7]

(5) Ab initio calculations of metal centers are not straightforward and are of limited use in parameterization. Inorganic density functional calculations are steadily increasing in number and may soon be very useful in determining metal-based parameters.

0009-2665/95/0795-2629$15.50/0

(6) Many bioinorganic molecules are extremely flexible and can adopt a large number of conformations.

(7) Most bioinorganic systems, especially metalloproteins, are fairly large. Although MM is a simple method, the calculations for molecules of this size are computationally intensive and require a number of approximations.

(8) Partial charges around metal ions are not easily obtained, and although they are often ignored in inorganic MM, their importance in bioinorganic MM is still being debated.[8,9]

Before reviewing bioinorganic MM calculations I would like to give a quick overview of MM calculations and discuss some of the problems that are of specific importance in inorganic and consequently also in bioinorganic MM.

II. Molecular Mechanics

In molecular mechanics (MM), mathematical equations are used to simulate all the components that contribute to the strain energy of a molecule, which is then minimized to find a low-energy conformation (local minimum). Different force fields use different mathematical equations, and thus parameters, to simulate the various interactions that describe a specific geometry on the potential energy surface.[10] This potential energy hyperspace has $3N + 1$ dimensions where the position of N atoms in the molecule are responsible for $3N$ of the dimensions, and an extra dimension is defined by the energy.

Typically, the equations used in a valence force field are a function quantifying the strain present in all bonds

$$V_{\text{bond}} = \sum {}^1/_2 K_r (r - r^\circ)^2 \quad (1)$$

a bond angle function

$$V_{\text{bend}} = \sum {}^1/_2 K_\theta (\theta - \theta^\circ)^2 \quad (2)$$

a function that calculates all the dihedral strain

$$V_{\text{dihedral}} = \sum V/2[1 + \cos(n(\theta + \theta_{\text{offset}}))] \quad (3)$$

and a number of nonbonded terms, such as the Lennard-Jones potential function that describes van der Waals interactions

$$V_{\text{vdw}} = \sum [A_{ij}/R^{12}{}_{ij} - B_{ij}/R^6{}_{ij}] \quad (4)$$

a Coulombs law-like expression that treats the electrostatic interactions

$$V_{\text{estat}} = \sum (q_i q_j)/(\epsilon R_{ij}) \quad (5)$$

and an out-of-plane deformation term

$$V_{\text{oop}} = 0.5 k_{\text{oop}} \delta^2 \quad (6)$$

In order to use these equations to calculate the total strain of a molecule one needs to know the force constant (K) for all the bonds, bond angles, and out-of-plane deformations in the molecule. Also required are the ideal bond lengths (r°) and bond angles (θ°),

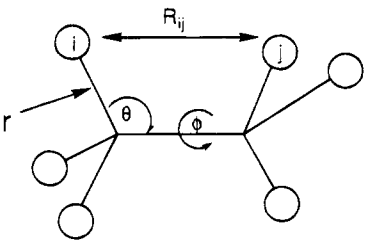

Figure 1. Parameters used in a molecular mechanics force field.

the periodicity of the dihedral angles (n), the barriers to their rotation (V), and if out-of-plane deformations are used, the angle between the plane defined by three atoms and the vector from the center of these atoms to a fourth bonded atom (δ). The van der Waals parameters (A_{ij}, B_{ij}) between the ith and jth atoms are necessary to simulate the nonbonded van der Waals interactions, and finally, the point charges (q_i and q_j) and the effective dielectric constant (ϵ) are needed to model the electrostatic potential. Figure 1 illustrates the most important interactions that are evaluated to define the potential energy surface.

III. Inorganic Molecular Mechanics

The earliest inorganic MM calculations were based on the idea that isomers with the least short, high-energy, nonbonded interactions would be the preferred isomers,[11-15] and therefore only the van der Waals forces were considered. Clearly, this is a rather crude approximation, as the bond lengths, bond angles, and torsional angles can be deformed to accommodate the high-energy nonbonded contacts. In order to find the low-energy structures, the next generation of calculations systematically adjusted the angles, lengths, and torsions while monitoring the nonbonded interactions.[16-18] This process has since been perfected by the addition of minimization routines in the current generation of MM programs.

Inorganic molecular mechanics have recently been reviewed.[19-27] Most inorganic compounds consist of an organic ligand and a metal. Since we can assume that the interactions of the organic backbone are not greatly altered by metal coordination, and since the organic moiety can easily be modeled with existing organic force fields, these are usually modified and used in inorganic MM. The vast majority of inorganic MM calculations use organic force fields and derive parameters for the interactions involving the metal ions by systematically fitting crystal structures with calculated structures. The torsions around the metal, as well as the van der Waals, and electrostatic interactions of the metal are usually ignored.

SHAPES, a new force field designed specifically to model the large variety of coordination geometries found in transition metal complexes, has recently been released. The metal parameters were derived by a combination of quantum mechanical calculations, solid-state structure, and normal coordinate analysis.[28]

IV. Bioinorganic Molecular Mechanics

We can consider bioinorganic MM an offshoot of inorganic MM as the major problems are the same,

and the methods used to overcome these difficulties are identical.

A. Bioinorganic Parameters

Most MM programs are capable of routinely analyzing commonly occurring organic functionalities, including peptides and nucleotides. However, they are incapable of routinely doing accurate inorganic and bioinorganic MM calculations. Parameters for the metal and its nearest neighbors need to be derived and added to the force fields before any calculations can be undertaken. In some cases the programs themselves have to be further modified to overcome difficulties such as the unique labeling problem, which is described in section IV.A.iv.

i. Obtaining Parameters by Structure-Based Optimization

By analogy to inorganic systems, bioinorganic molecules consist of a metal bound to organic ligands, peptides, or nucleotides, and thus existing organic and biochemical force fields (e.g. MM2,[5] AMBER,[29] MOMEC,[30] CHARMm,[31] DREIDING[32]) are modified to include metal parameters.

The procedures used to obtain the parameters for the metals and their coordinated atoms are identical to those used in inorganic MM. In section V of this review I have tried to summarize all the bioinorganic MM papers published before 1995. Wherever possible I have included details on how the parameters for the metal and its closest neighbors were obtained. In the vast majority of the studies, the parameters were derived by "interpolating" from a number of known crystal structures. The procedure that is generally followed involves finding crystal structures of compounds with the same metal in the same oxidation and spin state, and in a similar coordination environment. These solid-state structures are then minimized with an initial set of metal parameters that have been added to a well-established force field. The preliminary guesses are normally based on published parameters for similar metals, or for the same metal in a different coordination sphere, or from different force fields. Hay's inorganic MM review[21] gives a thorough listing of all the available metal parameters, their sources, and associated force fields. The initial metal parameters are refined by systematically varying them and comparing the calculated structures with the solid-state structures, until a satisfactory agreement between the two has been achieved. Once a new set of parameters has been obtained in this manner, it is good practice to test the modified force field on related crystal structures that were not used in the fitting.

Obviously, the quality of the parameters depends on the number of crystal structures used in the parameterization, and the relationship between the structures used in the derivation, and the system that is to be studied (interpolation vs extrapolation). The fit between the calculated and the solid-state structure can be assessed by determining the root mean squared standard deviation between the x, y, and z coordinates of all the non-hydrogen atoms, by comparing the internal coordinates, or by measuring some other geometric property of interest, such as the degree of ruffling in porphyrins. The torsions around the metal are usually set to zero and electrostatic effects are often ignored (see section IV.A.v). Force fields modified in this manner have been shown to be very reliable predictors of solid-state geometries. However, their utility at modeling systems in solution or thermodynamics is questionable. This is not surprising, since in essence they produce a "crystal-averaged" model.

In most force fields a number of different parameters are used for the same internal coordinates, depending on their environment, e.g. different C–O ideal bond lengths and force constants can be used for alcohols and ethers. A common approach to modeling bioinorganic systems is to develop specialized parameters for the system of interest, e.g. iron parameters for transferrin,[33] or cobalt(III) parameters for cobalt bleomycin.[34] The advantage of this approach is that the results are more accurate, but on the other hand, the parameters need to be derived on a system by system basis and are only useful for the systems for which they were established.

ii. Universal Force Fields

Universal force fields, such as the UFF[35] and DREIDING,[32] use the opposite approach, the force constants are based on the atom type and its hybridization, not on its environment. Obviously some accuracy is lost, but parameterization is simpler, and the field can be used to make predictions for novel combinations of elements. The DREIDING force field has been very successfully modified in order to model nonplanar distortions in tetrapyrroles. The modifications were based on the normal coordinate analysis and structure-based optimization of nickel(II) octaethylporphyrin complexes.[36,37]

iii. Electronic and Other Effects

Special care needs to be taken with the electronic effects due to the partially filled d orbitals of the metal. In the interpolation model they are implicitly incorporated in the parameters as these are obtained by interpolating a series of crystal structures with similar electronic effects. The multiple geometries available to the metal (square planar, tetrahedral, octahedral, etc.), the charge and spin state, and, if present, the trans and Jahn–Teller effects need to be considered. For example, we have added an additional function to the MOMEC force field to model Jahn–Teller effects in $Cu–N_6$ compounds.[38]

iv. The Unique Labeling Problem

There are a number of ways that have been used to overcome the problem of the variable geometries around the metal. The most common method assigns an ideal ligand–metal–ligand (L–M–L) angle based on the geometry around the metal being investigated e.g. ideal angles of 180° and 90° in a square planar system. This method has two drawbacks, the coordination around the metal (e.g. square planar) is predetermined by the parameterization, and in complexes with equivalent coordinating ligands one has to distinguish between those L–M–L angles that are 90° and those that are 180°. This multiple reference problem has been solved in a number of ways; a subroutine that minimizes the L–M–L angle to the

closest ideal angle has been used;[39] a trigonometric function has been added to the L−M−L angle deformation function (eq 2) so that the function has multiple minima;[28,30,32] and special substructures have all been used to differentiate one set of L−M−L angles (e.g. ideal angle 90°) from another (e.g. ideal angle 180°).[40] A more realistic way to model the L−M−L angle has been to use the bond angle deformation function (eq 2) for all the angles except those around the metal, which are handled by 1−3 Urey−Bradley nonbonded interactions.[20,41] This allows the metal to adopt the coordination geometry most favorable to the complex not limiting it to a preconceived coordination geometry and has the advantage that only the bonding parameters for each type of new metal−ligand fragment modeled need to be derived.

v. Charge

The use of integer formal charges on metal ions has been shown to be unrealistic as the metal charge is partially spread out to the neighboring ligands. A number of approaches to overcome this problem and to model the transition metal−ligand electron distribution have been used.

The exclusion of explicit electrostatic terms is a very common way to avoid the problem in inorganic MM calculations,[19,25] and this approximation has also found applications in bioinorganic calculations.[42,43] It has been argued that inclusion of electrostatic terms does not affect the structure, but it does have a considerable influence on the molecular energies.[44]

There is some disagreement whether charge effects are required in modeling bioinorganic compounds. On the basis of his analysis of zinc coordination in carbonic anhydrase, Vedani[8,45] suggests that electrostatic effects involving the metal ion are not as important as previously thought. However, Merz,[9] studying the same system, stresses the importance of charge effects.

Clearly, having no explicit electrostatic term in the force field does not mean that the electrostatic interactions are neglected, it mearly means that they are mixed into other functions.

Approaches using *ab initio* and semiempirical MO calculations to compute charge distributions for some small molecules have been successful but these involve, much in contrast to the molecular mechanics calculations, a major computational effort. The charges of the 20 standard amino acids and four nucleotides have been determined and are used as fixed charges in some force fields. Therefore, an alternative to calculating the partial charges on all the atoms in the molecule is to use the well-proven point charges for the ligand (amino acids and nucleotides) and fitting the metal charges.[33] Most methods that consider electrostatic interactions are based on fixed predetermined charges which do not respond to structural or environmental changes, instead the environmental effects are quantified by a bulk dielectric constant (ϵ), which is typically between 2 and 4 (see eq 5). A relatively simple approach has recently been developed, the charge equilibration approach, which calculates charge distributions analytically, using the geometry of the system and experimentally available atomic parameters such as the atomic ionization potentials, electron affinities, and atomic radii.[46] The advantages of the charge equilibration approach are its simplicity and the fact that the charge can be calculated as a function of the geometry. This method has been used in the modeling of porphyrin ruffling, where addition of the partial charges resulted in more accurate relative energies, but did not lead to any significant structural changes.[47] A disadvantage of the method is that it does not conserve charge within defined regions, such as a charged protein side chain.

vi. Conformational Searching

In the vast majority of published inorganic and bioinorganic molecular modeling studies no conformational searches have been conducted. There are two reasons for this: (1) Coordination of a ligand to a metal constrains the ligands flexibility, and subsequently the number of conformations available to the metal ligand system are reduced. (2) Methods using internal coordinate frames (torsion angles) are complicated by the number of adjacent cyclic systems formed by metal−ligand complexation.

An excellent comparison of methods employed in conformational searching in organic molecules has been published,[48] and a similar study needs to be undertaken for inorganic/bioinorganic complexes.

The energy minimization routines employed by all MM programs refine the starting geometries to local minima, which may not be the global or lowest energy minima. The aim of a conformational search is to find as many minima as possible, which hopefully includes the global minimum, and to compute the Boltzmann population. In doing such a search, a large number of high-energy starting conformations are generated, which are then minimized, compared with previously found conformers, and stored if they are unique.

For a thorough search the crude starting geometries need to be spread all over the potential energy surface because if only part of the surface is covered one cannot be sure that all important low minima will be found. Three methods can be used to generate the high-energy geometries: (1) deterministic or grid searches that cover all areas of the conformational space systematically, (2) stochastic or Monte Carlo methods, which use a random element to generate starting geometries, and (3) molecular dynamics. The systematic searches cover all areas of the conformational space; however, for large or flexible molecules the cpu time required is prohibitive.

Common stochastic methods are the random kick method[49] and the torsional Monte Carlo method.[50,51] The two methods differ in the coordinate system in which they operate. The torsional Monte Carlo method uses internal coordinates, while the random kick method uses external coordinates. The advantage of using internal coordinates is that they cut down the molecular degrees of freedom. It is well-known that all the bond angles and distances do not change much between all the different conformations of a molecule, and that the main changes are in the torsional angles.[52] For this reason it is the torsion angles that are varied to obtain the crude starting

geometries in the Monte Carlo search. In each Monte Carlo step a random number of torsional angles are varied by a random amount generating a new starting geometry that can be minimized. For cyclic systems the ring needs to be cleaved at one point so that all the other torsions can be varied. To prevent the two ends of the cleaved ring from being too close or too far from each other, a ring closure constraint is set. The situation is more complicated for bioinorganic systems where coordination often results in a number of adjoining cyclic rings.

In the Cartesian stochastic (or kick method) search method[49] a random kick is applied to each atom in the molecule, generating a new high-energy starting geometry for energy minimization. The advantages of this method are that it can be applied to bioinorganic systems just as easily as to organic systems, and that it requires only eight lines of Fortran to implement.

Molecular dynamics involves the calculation of the time-dependent movement of each atom in a molecule. This is achieved by solving Newton's equation of motion. Dynamics is efficient at exploring local conformational space but it is not effective at crossing large energy barriers and thus it is not suited for searching globally. To favor faster and more complete searching, high temperatures can be used. However, sampling structures during a high temperature run usually results in a larger proportion of high-energy conformers and should be used with caution. In order to prevent the molecular dynamics search from going to areas of the potential energy surface that have already been searched, a penalty can be assigned to sampled points.[53]

In order to cross large energy barriers during a stochastic dynamics simulation, MacroModel v 4.5 has a mixed-mode Monte Carlo/Stochastic dynamics. In such a simulation a Monte Carlo torsional variation is performed every N time steps, where N is selected by the user.[54]

To date, the vast majority of bioinorganic molecular mechanical studies have not included a conformational search. Instead it is common practice to enter all probable structures individually and minimize them separately, or to minimize the one structure and ignore all other possible conformations. The possible structures are generated by drawing all possible combinations of the chair, boat, and skew-boat conformers for six-membered rings, and the λ and δ conformers for five-membered rings. Isomers and stereoisomers are handled in the same way. For example, Raos[55] in his work on the stereochemistry of N-alkylated amino acids minimized 19 possible conformations of the chelate rings in bis(L-*N*,*N*-dialkylalaninato)aquacopper(II).

Using a conformational search to find all the possible conformations is faster and more accurate than entering individual conformations. Drawing all the possible conformations is a tedious process. More importantly, by generating probable conformers one can easily miss the global minimum or other important low-energy conformations, especially in cases where the chelate conformations are far from the ideal conformations. In larger inorganic compounds, like coenzyme F430[56] and cobalt bleomycin,[57] the many available low-energy minima make molecular mechanics meaningless without a conformational search.

vii. Solvation

In section V, which summarizes all the bioinorganic calculations done to date, I have included details of the solvation treatment, if the solvent was considered. In the vast majority of cases the MM force fields were parameterized on the basis of solid-state data, i.e. structure-based optimization, and the minimized structure approximates a "crystal-averaged" conformation. There is no doubt that other environmental effects which are not implicit in "crystal-averaged" parameters, especially solvent effects, are of importance in bioinorganic chemistry and that these need to be considered. The obvious solution of using a large number of explicit solvent molecules is too computationally intensive to be of general use, and solvation effects have been ignored in the vast majority of studies. The self-analytical GB/SA treatment proposed by Still[58] and implemented in MacroModel has been used in some studies.[33] Although this approximation does not require excessive amounts of computer time, it does require knowledge of the charge distribution.

viii. Ideal Hole-Size Determination

The effect of varying the metal size on the conformation of a bioinorganic molecule can be determined by molecular mechanics. This has been particularly useful in porphyrin chemistry. A lively debate on the merits and demerits of using excessively strong force constant[59] and systematically varying the ideal bond length, as opposed to using standard force constants[60] has been ongoing. Unfortunately, the most accurate method, that is mathematically fixing the bond lengths by using Lagrange's multipliers,[61-63] is only possible if full matrix second derivative methods are used and is only implemented in a limited number of programs.

V. Systems Analyzed by Bioinorganic Molecular Mechanics

A. Complexes of Amino Acids

The modeling of amino acid complexes is important because these complexes can be viewed as the building blocks of metalloproteins, which means their modeling is a starting point for obtaining parameters to analyze large biomolecules.

The pioneering bioinorganic molecular mechanics calculations by Buckingham, Sargeson, and Snow[64] on the molecular geometry and relative stabilities of cobalt(III) triethylenetetramine-(S)-prolinato complexes were the first bioinorganic MM analyses to be published and the first inorganic MM calculations to vary all the independent internal coordinates simultaneously. The geometries and relative stabilities of the isomers that were obtained were in good agreement with experimentally obtained data. This and subsequent investigations of cobalt(III) triethylenetetramine glycine complexes,[65-67] were intended to

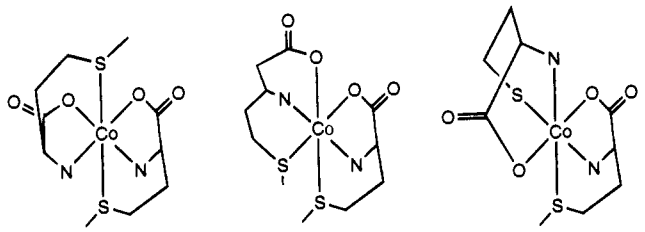

Figure 2. The three geometric isomers of bis(L-methionato)cobalt(III).

determine the detailed stereochemistries and relative stabilities of polyamine metal complexes.

The three isomers of bis(L-methionato)cobalt(III) shown in Figure 2 have been characterized by X-ray crystallography and analyzed by MM,[68] using the MOMEC force field.[30] The strain energies of all three geometric isomers (Figure 2) with all possible configurations around the sulfur atoms (i.e. *SS*; *RS*; *RR*) were calculated. The resulting geometries were consistent with the solid-state structures. Furthermore, the strain energies of the most stable configuration of all the isomers were very similar, indicating that a nearly equal mixture of the three would be expected, as was observed experimentally.

In the past 20 years MM have often been used to study stereoselectivity in inorganic systems. Brubaker[69] was one of the first to be interested in this phenomena and analyzed mixed-ligand complexes of cobalt(III) with a flexible tetramine ligand and glycine or alanine.

A recently modified MM2 (87) force field has shown better agreement with the crystal structure of tetrahedral zinc complexes of cysteine, histidine, and glutamic acid derivatives than those obtained using the modified neglect of differential overlap (MNDO) method.[70]

The conformation of the (*S*-glutathionato)(terpyridine)platinum(II) ion has been determined by a combination of MM calculations and two-dimensional NMR spectra.[71] By using a viscous solvent and low temperatures the authors were able to slow the correlation time of the (*S*-glutathionato)(terpyridine)-platinum(II) ion, so that its NOE's could be measured. Constraints based on the NOE's were used in MM and molecular dynamics. Ideal bond lengths and angles involving platinum(II) were taken from the solid-state structure of a closely related platinum-(II) complex and were added to the CHARMm force field.[31] Force constants were obtained from infrared spectra.[72] No mention of any attempts to test the validity of these modifications is made. A starting structure for the molecular dynamics runs was generated with CHARMm. This structure was exported to the XPLOR program where an annealing procedure with the NOE distance restraints was set up. The 10 structures with the lowest rms deviation from the NOE distances were exported to CHARMm and minimized. They all minimized to the same final structure.

Modeling copper(II) complexes is complicated by the multiple and distorted stereochemistries the metal ion can adopt, as well as the Jahn–Teller distortions that occur. Raos and co-workers have

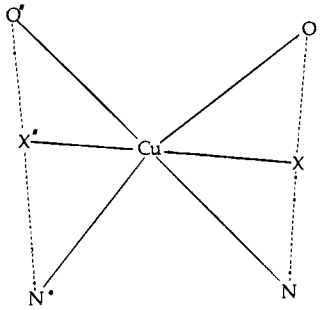

Figure 3. An additional bond angle function, with an ideal X–M–X* angle of 180°, can be added to a force field to model copper(II) distortions. The dummy atoms X and X* are added so that MX* bisects the angle O*–M–N* and MX bisects O–M–N, where the atoms marked with an asterisk (*) belong to the same ring.[76,81]

been modeling copper complexes of α-amino acids, as well as their N-alklyated and N,N-dialkylated derivatives for more than 10 years. In order to simulate the plasticity of tetracoordinated copper(II) complexes with valine,[73–76] isoleucine,[77–78] glycine,[79] alanine,[55] threonine,[80] and their derivatives, they have used six different MM models. To date, their main interest has been in establishing MM methods that are capable of modeling the structure of these complexes, and the stability differences between the bis-copper-(II) complexes of the natural and enantiomeric forms of amino acids. The emphasis has been more on finding a good model, rather than analyzing the complexes.

All models use out-of-plane deformation potentials for the carboxylate groups and aromatic rings. In order to keep the 4-coordinate complexes planar, dummy atoms were placed in the apical positions and the complex was treated as a pseudo-octahedral structure.[80] The thermodynamic stabilities of copper-(II) amino acid complexes were well modeled with dummy atoms; however, the coordination geometry was not predicted well. The apical dummy atoms were therefore replaced by a distortion potential to improve the geometric simulation. This was achieved by adding two new dummy atoms, such that the metal–dummy bonds bisect the N–Cu–O angles (Figure 3) and by using a bond angle function, such as eq 2, with an ideal dummy–metal–dummy (X*–M–X) angle of 180°.[76,81]

The model did not perform satisfactorily and so a two-well angle-bending potential, with minima at 109.47° and 180° for the N–Cu–N and O–Cu–O angles and minima of 90° and 109.47° for the N–Cu–O angles, was added to the distortion model. The shortcoming of this approach was that besides predicting the two minima expected for a CuN_2O_2 complex, it also predicted the presence of two "false" minima within 1–5 kJ/mol of the global minimum.[82] These same problems were encountered when an electrostatic model with two dummy charges above and below the plane was used together with a harmonic bond stretching function to model the bond between the copper and the dummy point charges.[83] The force constant for the bond between the metal and the dummy point charge and all the charges were systematically varied to obtain the best fit with the crystal structure. The fact that so many parameters are fitted on the basis of one crystal structure is cause

for some concern in evaluating this method. Some of the problems in these studies might be due to Jahn–Teller effects that were not considered.

In all the studies systematic searches were conducted to find all the minima. The models are fairly accurate; however, they parameterized on a limited number of copper(II) complexes, and due to the large number of parameters required they are not very useful as general methods.

B. Nucleotide Complexes

In the following section I will review some MM calculations involving nucleotide complexes. Additional studies of metal–DNA interactions are covered in the antitumor drug section (section V.D). Since a review of the computational modeling of DNA–metal interactions is currently being written,[84] I will be brief.

The metal binding sites, the metal–ligand stoichiometry, and the molecular geometry of complexes of the vanadyl ion (VO^{2+}) with the adenine nucleotides AMP, ADP, and ATP have been determined by a combination of EPR, ENDOR, and MM techniques.[85] The axial solvent (water)–vanadyl distance was constrained at 2.23 Å, so that a linear H_2O–V=O arrangement with a metal–(hydroxyl) proton distances of 2.92 Å was obtained, which corresponds to that determined by the ENDOR experiments. The nucleotides were bound to the metal ion through the α and β phosphate groups in the ADP and AMP-CP complexes, and through the β and γ phosphates in the ATP complexes. This binding arrangement was used because it corresponded with the metal–proton distances calculated from the ENDOR spectra. The complexes were minimized using the SYBYL[86] and INSIGHT[87] programs; however, no mention is made of what vanadyl parameters were used, and how they were obtained.

In order to model the inner- and outer-sphere complexes of chromium(III) nucleoside mono- and triphosphates, crystal structures of cobalt(III) and chromium(III) polyphosphate complexes have been used to determine metal parameters for the AMBER force field, by structure-based optimization.[88] Charges on the donor atoms and the metal ion were calculated by the CHELEQ program.[89] The crystal structures of nucleoside monophosphates were used as starting geometries for minimization and a brief conformational search was conducted by varying three critical torsional angles. The paramagnetic contribution to the relaxation rate for two of the proton signals of $[Cr^{III}(H_2O)_6]^{3+}$ adenosine 5′-monophosphate and $[Cr^{III}(H_2O)_6]^{3+}$ inosine 5′-monophosphate as determined by NMR, was compared to that calculated on the basis of the chromium–proton distance in the minimized structure. Semiquantitative results, vs NMR, were obtained by the MM calculations.

Barton's rhodium phenanthrenequinone diimine (phi) and phenanthroline (phen) metallointercalators have been computationally analyzed. A 13 residue oligopeptide has been coupled to a rhodium-intercalating complex, and its sequence-specific binding to DNA has been graphically analyzed[90] using Macro-Model.[51] NOE data have been used as a starting point for an MM minimization of $Rh(NH_3)_4phi^{3+}$ intercalated into a $d(TGGCCA)_2$ strand.[91] The Insight/Discover programs were used and charges were determined by AM1 calculations as described by Richards.[92] Distance constraints using a 50 kcal mol^{-1} $Å^{-2}$ force constant were applied for hydrogen bonds between base pairs and for the experimentally observed NOE contacts. During minimization the coordinates of the rhodium complex were fixed, and no metal parameters were needed. Intercalation was shown to occur from the main groove and the selectivity for the 5′-GC-3′ sequences was explained by the hydrogen bonds formed between the axial ammines of the complex and the guanine O6 atoms above and below the intercalation site.

Osmium tetraoxide bispyridine reacts readily with thymines in single-stranded DNA. It has been used to detect local changes, such as cruciforms, triplexes and B–Z junctions, in the double-helical structure of DNA. Standard AMBER parameters and charges were used to model the nucleotide fragments in the osmium tetraoxide bispyridine complexes with four B-DNA and one A-DNA strand.[93] The solid-state structure of the osmium tetraoxide bispyridine ester of 1-methylthymine was added to five DNA fragments to generate starting geometries. Atomic charges for this fragment were calculated with Gaussian-90.[94,95] Since no osmium parameters were available, the osmium atom, the coordinating atoms, and the C5 and C6 atoms in the modified thymine were held rigid during the calculations, while the remaining part of the complex was minimized.

C. Carbohydrate Complexes

Copper(II) complexes of D-arabinose, D-xylose, and their methyl glycosides were studied by ^{13}C NMR and MM.[96] MM2 was used; no parameters or further calculational details were given.

Experimentally determined NMR coupling constants have been compared with those derived by the Karplus equation using dihedral angles obtained from MM2-minimized cobalt(III) glucosamine complexes.[97] The default CACHE MM2 parameters for cobalt were used without regarding solvent effects or doing conformational searches. Reasonable agreement between experimental data and the calculated structures was obtained for rigid complexes; however, the more flexible systems were not modeled very well.

D. Antitumor Drugs

i. Budotitane

Budotitane, bis(1-phenylbutane-1,3-dionate)bis(ethoxy)titanium(IV), is a promising antitumor drug for which there is no crystal structure. This is probably due to the fact that no isomerically pure fraction can be obtained from the five possible isomers that are found in solution; see Figure 4.

The MOMEC force field[30] was successfully modified to reproduce the crystal structures and isomer distributions of analogous β-diketonato complexes of

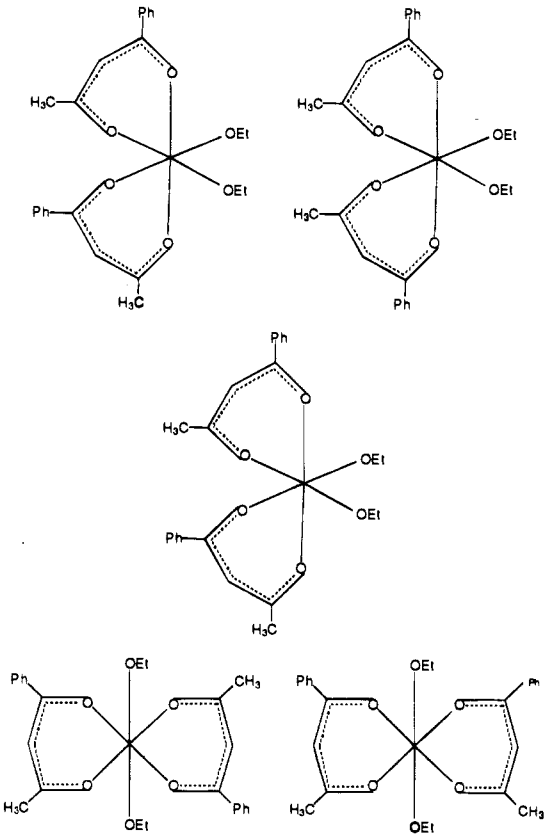

Figure 4. The five possible isomers of budotitane.

titanium(IV) and cobalt(III), and used to predict the geometry and isomer distribution of budotitane.[98]

ii. Bleomycin

The bleomycins (BLM's) are a family of glycopeptide-derived antibiotics which are used in the treatment of Hogkin's lymphoma; carcinomas of the skin, head, and neck; and tumors of the testes. In vivo it is proposed that Fe-BLM is the species responsible for strand scission, although other metallobleomycins can inflict DNA damage in vitro.[99-101] No crystal structure for BLM exists and the metal coordination sites are unknown. It is very important to know the details of the metal environment because the way BLM wraps around the metal determines BLM's shape and thus the site and selectivity of DNA binding.[102] To date, spectroscopic investigations of BLM and crystal structures of BLM analogues have been used to propose metal coordination sites. This has led to contradictory interpretations of the metal coordination sphere in BLM. The crystal structure of a Cu-BLM P3A, a BLM analogue which lacks the two carbohydrates, seems to suggest metal coordination through sites 1–4 and 6.[103-104] However, a recent NMR analysis[105-106] suggests that BLM binds the metal through positions 1–4 and 5; see Figure 5.

In order to analyze the two different coordination geometries, we have modified the MM2* force field,[51] for cobalt(III) bleomycin.[34] The new parameters were derived by structure-based optimization of cobalt crystal structures retrieved from the Cambridge Database, and tested on the crystal structures of cobalt BLM model compounds, e.g. PMAH in Figure 6A, that were not used in the parameterization.

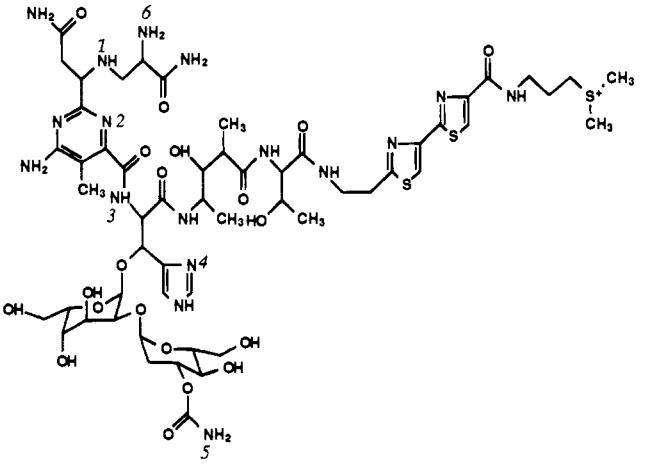

Figure 5. The structure of bleomycin.

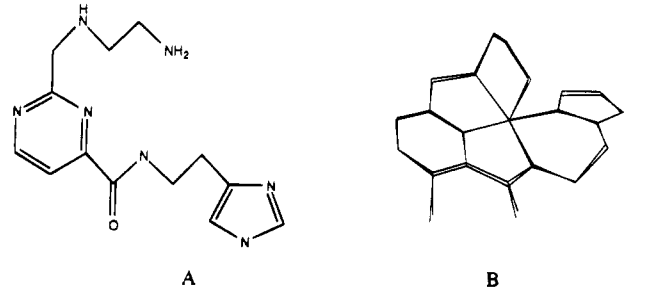

Figure 6. (A) The bleomycin analogue PMAH and (B) superimpostion of the calculated and solid-state structures of $[Co(PMA)]^{2+}$.

The structures of the BLM analogues were well reproduced (Figure 6B). An analysis of both binding geometries[107] showed that they were both sterically possible and that a change in the oxidation state of the cobalt will result in a geometric change. On the basis of BLM–DNA docking studies it was suggested that only the binding geometry involving metal ligation through the sugar residue (atom 5 in Figure 5) can interact with the minor groove of DNA, with both the bithiazole tail, and the metal-binding region of bleomycin (Figure 7). Extensive conformational searches were undertaken to find the energy minima. The DNA docking study was under taken with a fixed ideal decamer of DNA which was not refined.

On the basis of modeling studies of the BLM analogue Fe–PMA, it was suggested that intramolecular hydrogen bonding between the secondary amine group and the coordinated hydroperoxide could facilitate the O–O bond cleavage at the iron center of Fe–BLM's.[108] These calculations also confirmed that the binding geometry with the terminal NH_2 group axial is energetically preferred over that with an axial imidazole group; see Figure 8.

Nevertheless, it was presumed that hydrogen bonding of the secondary amine with a sixth ligand such as O_2 or O_2H^- would stabilize the form with an axial imidazole and make it energetically feasible. MM2MX was used with generic metal parameters and the energies of four conformers with the NH_2 axial and two conformers with the imidazole axial were calculated. Subsequent experimental work has shown that the secondary amine group of PMAH (and BLM) does not facilitate O_2 activation by hydrogen bonding.[109]

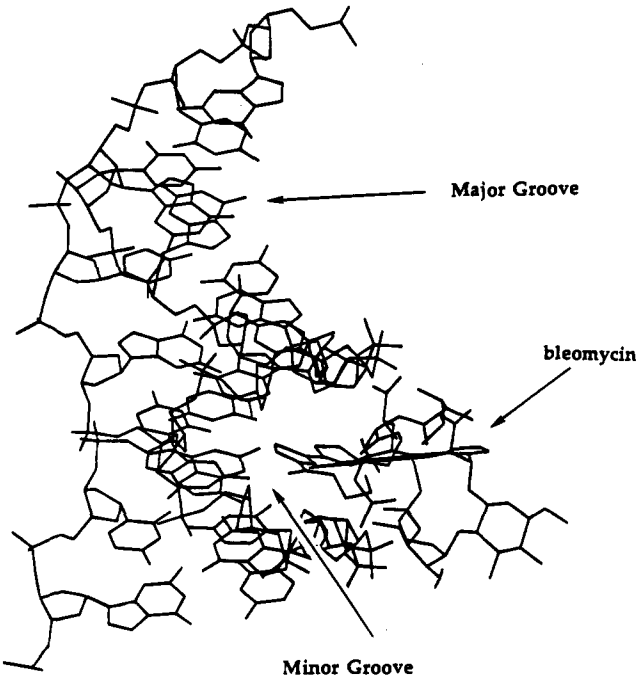

Figure 7. Binding of cobalt(III) bleomycin to the minor groove of self-complementary d(GCGCGCGCGC)$_2$. (Hydrogen atoms have been removed for clarity.)

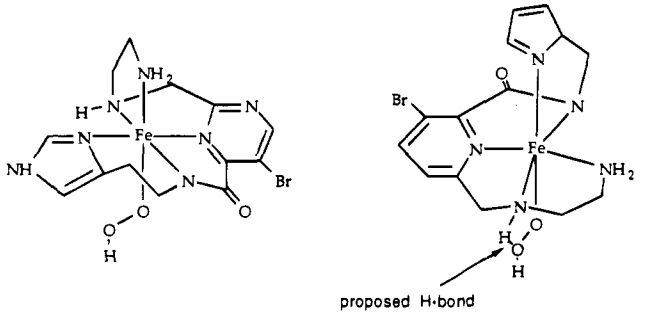

Figure 8. (A) Fe–PMA complex with the terminal amine group binding axially and (B) Fe–PMA complex with the imidazole group binding axially. The proposed hydrogen bond between the secondary amine and the hydroperoxo group is also shown.

iii. Platinum Antitumor Drugs

Due to their extensive use in anticancer therapy and the paucity of structural data, the binding of platinum complexes to DNA has been extensively analyzed by molecular mechanics. The majority of these complexes are square planar and have cis leaving groups and cis amine nonleaving groups with at least one hydrogen on each nitrogen. Cisplatin and carboplatin (Figure 9) are among the most commonly used anticancer drugs in the United States.

Upon entering the cell, one or both chlorine ligands are lost and the platinum binds to the DNA through the vacated coordination site(s). The preferred binding sites are the N7 atoms of guanine and adenine

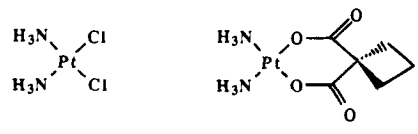

Figure 9. Structures of cisplatin (left) and carboplatin (right).

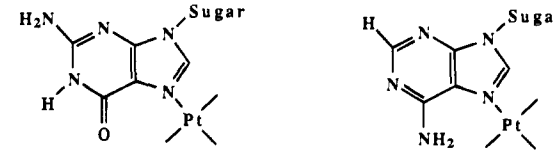

Figure 10. Preferred binding sites of cisplatin to DNA is through the N7 atoms of guanine and adenine.

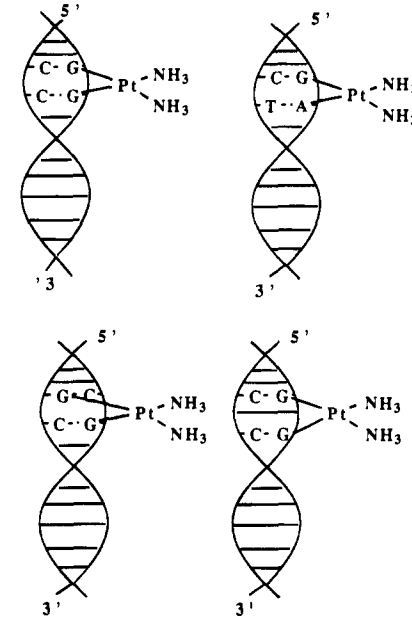

Figure 11. Inter- and intrastrand binding of cisplatin to DNA that is believed to be responsible for cell death.

(Figure 10). It is believed that the bifunctional complexes (Figure 11) between the platinum and DNA are responsible for cell death.

In a review entitled "What can be learnt from computer-generated models of interactions between DNA and Pt(II)-based anti-cancer drugs", Hambley has described and critically analyzed all the research in the field up to and including 1991.[110] In the paragraph below I have summarized some of this early work and added some of the computational details that were found in the original literature.

Using AMBER, with specially derived parameters and charges for the platinum complex and the coordinated guanines, it was found that the binding of cisplatin causes (i) a kink in the helix of DNA, (ii) a tilting of the two coordinated bases toward each other, (iii) a change in the conformation of the guanosine sugar, and (iv) the formation of a hydrogen-bonding network between the two amine ligands and the DNA.[111] The same parameters were used in NMR/MM studies of platinated decanucleotides. Correlation between the NMR data and modeling results revealed the existence of an equilibrium between several kinked structures.[112,113] A separately modified AMBER field was used to confirm NMR evidence for the existence of monomeric macrochelate complexes between platinum, the nucleotide base, and the DNA phosphate.[114] AMBER was also used to model *cis*-(1,2-diaminocyclohexane)platinum(II)[115] and hydrogen-bonding schemes in cisplatin.[116,117] Using the MOMEC program with modified AMBER parameters obtained by modeling small bis(nucleobase)-diamineplatinum(II) complexes,[118] the isomer pref-

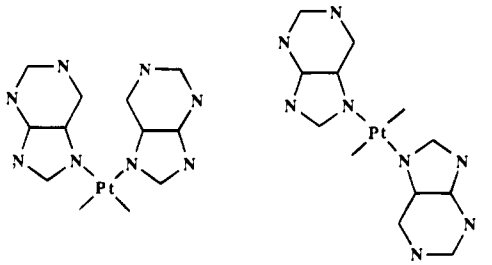

Figure 12. Head-to-head isomer (left) and head-to-tail isomer (right) of bis(nucleobase)diamineplatinum(II) complexes.

erence and ligand rotation barriers in bis(amine)-bis(purine)platinum(II) complexes were analyzed. Electrostatic charges for the nucleic acids were taken directly from the AMBER field, the charge on Pt was estimated as $+0.50e^-$ and for the amine hydrogens as $+0.20e^-$. Constraints were applied by using the method of Lagrange multipliers.[63] In general, it was found that the head-to-tail isomer was more stable than the head-to-head isomer (Figure 12) although there is some nucleobase dependence.

An analysis of the stereochemical factors influencing monofunctional and bifunctional binding to adenine and guanine has been reported using the same parameters. It was found that monofunctional binding of cisplatin results in base rotation of up to 20° and that bifunctional adducts with GpA sequences have a highly unfavorable contact between the NH_3 ligand and the NH_2 of the 3′-adenine.[119,120]

Recently, Kozelka[121] has used ab initio calculations to derive force field parameters for modeling platinum–adenine binding. Comparison of $[Pt(NH_3)_3(adenine)]^{2+}$ with $[Pt(NH_3)_4]^{2+}$ has shown that for platinum, adenine is a better σ donor than NH_3, but its capacity as a π acceptor is weak. Kozelka's modified AMBER parameters[111,121] were also used to model a 22 base pair DNA strand with a *cis*-platinum residue coordinated to two central guanine bases.[122] It was found that the intrastrand adduct bends the double helix by about 55° toward the major groove, that the double helix retains its average twist angle, and that the distortion is localized at the platinated d(GC/CG) sequence. These findings were supported by electrophoresis and chemical probe experiments.[122]

The reactants and products of the hydrolysis of cisplatin and substituted bis(ethylenediamine)dichloroplatinum(II) complexes (see eq 7), have been analyzed by molecular mechanics and extended Huckel calculations.[123]

$$Pt(en)Cl_2 + H_2O \rightleftharpoons [Pt(en)(H_2O)Cl]^+ + Cl^- \quad (7)$$

The chair and half-chair conformers as well as the δ, λ, and meso isomers of the platinum ethlyenediamine products and reactants were minimized with MMX in both tetrahedral and square planar geometries.[123] The values and origin of the metal parameters are not reported. The complexes were constrained to a square planar geometry by fixing the donor atoms to the xy plane. (One has to presume L–Pt–L angles were not defined.)

Hambley and co-workers have been using molecular modeling methods to design enantiomeric platinum complexes that would establish whether the

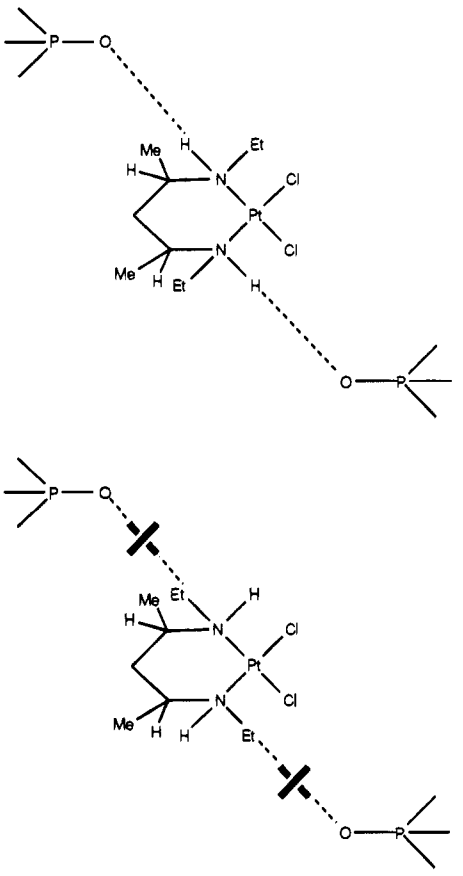

Figure 13. Intrastrand hydrogen bonding of the *RR,RR* conformation of $[Pt(eap)Cl_2]$ (top) and lack of hydrogen bonding with the *SS,SS* conformation (bottom).

absence of platinum GpA adducts is due to hydrogen bonding that cannot occur between the NH_3 ligands and a phosphate oxygen on the 5′ side of the adduct, or whether it is due to the loss of the hydrogen bond between the NH_3 ligands and exocyclic oxygen of the guanine on the 3′ side.[124] Modeling studies suggested that the *RR,RR* conformation of $[Pt(eap)Cl_2]$ would form an intrastrand hydrogen bond while the *SS,SS* conformation would not; see Figure 13. This prediction has yet to be confirmed, as the proposed synthesis of the *RR,RR* conformer resulted in the *RR,RS* conformer.[124]

Recently, van Houte[125a] has used Kozelka's modified AMBER force field[121] to model the solution structure of a 13-residue oligonucleotide containing a Pt–GTG adduct. The structure of the DNA strand was built with an idealized right-handed B conformation, and the platinum was bonded to the N7 atoms of the guanines. The hydrogen bonds between Watson–Crick base pairs involved in forming the Pt–GTG adduct were included/omitted in the MM calculations, on the basis of NMR studies. Two very different starting structures were used, both were minimized. NOE distance constraints were added and the structures were reminimized before running two 10 ps molecular dynamics simulations, the first at 500 K and the second at 800 K. The energy-minimum structure was found by releasing the NOE constraints and minimizing the structures which resulted in no additional conformational changes. It was found that the structural distortion caused by complexing platinum is very local and is predomi-

nantly caused by conformational changes induced by the guanine on the 5′ side of the *cis*-Pt−GTG adduct. This can explain why the 5′-*cis*-Pt−G of *cis*-Pt−GTG is a hot spot for base substituted mutations. The degree of unwinding at the platinum binding site and a kink of 20° were also calculated.

A previously modified AMBER[125c] has been further modified (by structural optimization) for simulating platinum amine/ammine complexes of guanine derivatives bound via N7.[125b] Solvent and counterion effects were modeled with a distance-dependent dielectric ($\epsilon = 4r$) and partially neutralized phosphates. The structural features were in good agreement with X-ray crystallographic and NMR results, and the relative stabilities of the head-to-head and head-to-tail conformers conformed with those determined experimentally.

E. Siderophores and Synthetic Mimics

Siderophores are organic iron chelators, produced by microorganisms to regulate iron transport and concentration. Gallo and co-workers have been studying these systems since 1990.[126-128] They have used a modified MM2 force field in which the ideal lengths and angles were derived from a small number of crystal structures, and the force constants were derived from infrared spectra.[127] A Hill function with a formal charge of +3 on the iron and −1 on the charged oxygens was used to model the van der Waals interactions. The value of ϵ and the torsional parameters were obtained by using the phosphorus MM2 parameters for Fe(III). The parameters were tested by recalculating the crystal structures of iron(III) trencam and EDTA.[128] The strain energies of the bidentate ligands catechol, hydroxamate and oxalic acid were compared. These results should be treated with caution, as force fields derived directly from crystal structures cannot be used for thermodynamic comparisons of molecules with different functionalities. The strain energy of a siderophore mimic with a varying number of methylene units was calculated.[126] The results have not yet been experimentally confirmed.

F. Technecium Imaging Agents and Their Rhenium Analogues

Rhenium(V) oxo complexes are excellent structural models for radioactive ^{99m}Tc complexes. N_3S and N_2S_2 ligand systems have been structurally analyzed due to their use in radiopharmaceuticals. The AMBER force field was modified, by structure-based modification, to accommodate rhenium(V) and therefore ^{99}Tc.[129,130] The field was used to model rhenium complexes in which the carboxyl groups were deprotonated, because these species approximate those found *in vivo* . Attempts at drawing a structural correlation between the oxo−carboxyl distance and renal clearance were made.[129] Solution NMR, MM, and crystallography data were all consistent in their prediction of the binding geometry and protonation

$ReOECH_3$ $ReOTMECH_3$

Figure 14. Rhenium(V) oxo complexes of ECH_6 and $TMECH_6$.

state of the carboxylate side chains in the rhenium(V) oxo ligands ECH_6 and $TMECH_6$ (Figure 14).[130]

G. Metalloproteins

Metalloenzymes are very large and they cannot be analyzed in the same way as described for most of the other bioinorganic molecules reviewed here. Some approximations need to be made, these usually consist of limiting the MM analysis to the area of interest, which is normally the active site of the metalloprotein.

i. Carbonic Anhydrase

Carbonic anhydrase (CA) is a zinc-containing enzyme consisting of 260 amino acids, and it catalyzes the reversible hydration of carbon dioxide to bicarbonate. The YETI program, which employs directional potential functions for hydrogen bonds, has been used to refine the conformation of human carbonic anhydrase II (HCA II) with its natural substrate, bicarbonate, and with three heterocyclic sulfonamide inhibitors.[8] The crystal structure of HCA II has been determined with a resolution of 2.1 Å and was used as a starting point for the minimization. The structure of the substrate and inhibitors were taken from the Cambridge Crystallographic Data File[131] and graphically fitted into the receptor site. Only the active site, which is made up of 368 atoms, and the substrate were refined. Nevertheless, with standard cut off distances, this still generates about 23 000 nonbonded interactions. The metal−ligand interactions, that is a zinc atom coordinated by three histidine nitrogens and a water oxygen, were modeled by a combination of electrostatic and van der Waals contributions. Fixed dielectric constants, ϵ = 1.0, 2.0, 4.0, and 8.0, and distance dependent dielectric constants $\epsilon = r$, $2r$, $4r$ were used; $\epsilon = 4r$ was found to be most effective. The calculations were carried out with all the atomic charges set to zero. The results were surprisingly good and allowed the authors to conclude that the importance of electrostatic contributions in MM have been overestimated and no serious errors are introduced when these contributions are set to zero. In a second study by the same authors, directional potential functions for the metal interactions were added to the YETI program.[45] This allowed them to model the coordination changes that occurred upon substrate and inhibitor coordination to zinc. Fifteen different sulfonamide−CA complexes were minimized, seven preferred a trigonal bipyramidal geometry, three preferred a square planar geometry, and less than 1.0 kcal/mol separated the two 5-coordinate geometries for the remaining five complexes. In 1990 the

YETI program was modified once again and a new potential function was added to model metalloproteins.[132] The function includes variables for ligand–field stabilization, metal–ligand distances, metal symmetry, the directionality of the metal–ligand bonds, and ligand–metal charge transfer. The field was used to simulate the metal coordination, solvent interaction, and H-bond network formation of the native, complexed and cobalt(II) substituted human carbonic anhydrase I. Two zinc bound, 16 internal, and 485 surface explicit water molecules were generated by the SOLVGEN program[133] and included in the minimizations. The simulations were in good agreement with ab initio[134] and C^{13} NMR studies of HCA.[135]

In order to clarify the principles governing the interactions between CA and deprotonated benzenesulfonamides, MM calculations of the free molecules and the bound complex of CA and 20 benzenesulfonamides were performed with AMBER.[136] The anionic sulfonamides were optimized by the semiempirical molecular orbital AM1 method[137] and the partial charges obtained were used in the force field. It was found that while various methods of computing atomic charges gave different results, they all correlated strongly with each other. A distance-dependent dielectric constant ($\epsilon = 4r$), as was described in the previous study, was used. Starting structures were taken from the Protein Data Bank.[138] Clearly, only part of the molecule could be minimized, and a conformational search was out of the question. In place of a conformational search several orientations for the inhibitors in the active site were generated by graphic methods. All the amino acids in the first and second layer of the active site were minimized together with the substrate. The binding energies, E_B, were calculated using eq 8

$$E_B = E_{CA-S} + E^D{}_S + E^D{}_{CA} \quad (8)$$

where E_{CA-S} is the total interaction energy between the substrate and enzyme, $E^D{}_S$ is the distortion energy of the substrate calculated with respect to the optimized energy of the free substrate, and $E^D{}_{CA}$ is a measure of the conformational energy change induced in CA by the substrate binding. Analysis of the binding energy revealed that the difference in binding energies is largely due to short-range van der Waals forces and not the electrostatic interactions, and that the enzyme does not undergo substantial conformational changes upon binding the substrate. Although 60% of the E_{CA-S} value is due to the zinc–sulfonamide interaction, it is not responsible for the varying inhibitory behavior exhibited by different sulfonamides. The role of the zinc is thus presumed to be in attracting the anionic ligand to the active site.

In contrast to Vedani,[8,45] Merz[9] used a bonded approach to model CA. Although this limits simulations involving coordination changes around the metal, the authors argue that insufficient experimental evidence exists correlating energy changes with structural changes, and consequently they used a bonded approach with carefully determined partial charges. The AMBER force field was used to model

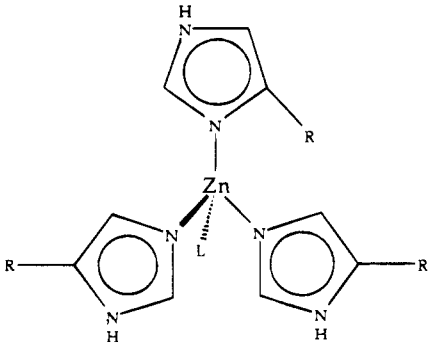

L = H_2O and OH

Small model: R = H
Large model: R = $CH_2CH(COCH_3)(NHCOCH_3)$

Figure 15. The "large" and "small" models used to calculate partial charges around the active site of carbonic anhydrase.

the zinc–water and zinc–hydroxide intermediates proposed in the enzymatic action of CA. In this work the authors have used what they have termed the large and small model of the CA active site (Figure 15) to calculate the electrostatic potential charges by MNDO[139] and ab initio methods. An enzyme model, the Zn^{2+} model, in which the zinc was assigned a formal charge of +2 and the charges on the oxygen and hydrogen in the hydroxide were based on ab initio calculations at the 6-31G* level, with the remaining charges set at the standard AMBER values, was also investigated. The starting structures were taken from crystal structures and crystallographically determined waters were used. By comparing the minimized structures with the corresponding crystal structures it was found that the large and small models produced better structures than the Zn^{2+} model, and that the Zn^{2+} model and the nonbonded approach produced significant error in molecular dynamics equilibration. Furthermore, it was found that the small model produced better results than the large model. The reason for this is not known.

ii. High-Potential Iron Sulfur Proteins

High-potential iron sulfur proteins (HiPIPs) contain a Fe_4S_4 cluster with a reduction potential between of +50 mV to 450 mV for the $[Fe_4S_4]^{3+}/[Fe_4S_4]^{2+}$ redox couple. The function of HiPIPs are not known; they have a very low degree homology and yet have very similar spectroscopic properties. The amino acid sequence for the protein from *Chromatium vinosum* is known; its crystal structure is available at a 2.0 Å resolution; and NOE data providing NOE connectivities for most of the protein, especially around the cluster, has been published. A molecular dynamics simulation of the protein was in much better agreement with the NOE data, than with the crystal structure.[140] The simulations were carried out with the AMBER program. Partial charges for the iron atoms in the reduced form of the protein were taken from the average charge of the two irons in 2Fe–2S

ferredoxins, which were determined from an ab initio SCF calculation by the same authors. The charges on the coordinated sulfurs were taken from the same study. For the oxidized form of the cluster 0.125 electrons were withdrawn from each iron and each coordinated sulfur in the cluster. It was found that minor changes in the charge distribution had little effect. This is not surprising since the structural features of most redox proteins do not change with a redox change of one. However, the cluster collapsed when the formal charges were used. The crystal structure with 75 crystallographic waters was used as the starting structure. In this and other studies it has been found that the force constants obtained from infrared spectra are about half the value required.

iii. Transferrin

Serum transferrin is an iron transport protein that binds Fe(III) and denies essential iron to invading bacteria. It contains two iron binding sites that coordinate the ferric ion through two phenolates of tyrosine residues, a carboxylate group of an aspartic acid, a histidine imidazole group, and through the two coordination sites of a bidentate carbonate ion. Although no MM analysis of transferrin has been published yet, a force field that has been developed for this purpose has recently appeared in the literature.[33] AMBER parameters for nonheme, high-spin iron(III) were derived from fitting three crystal structures, by statistically analyzing 44 iron(III) solid-state structures, and by analyzing other transition metal force field parameters. One of the crystal structures that was fitted was that of the iron complex of ethylenebis(*o*-hydroxyphenylglycine), EHPG. This structure was used as the UV, the charge-transfer and Raman spectra of Fe(III) EHPG are similar to that of transferrin. Iron(III) EHPG has two chiral centers and there are three different possible conformers (see Figure 16).

The three conformers were studied in vacuo, with a distance-dependent dielectric constant $\epsilon = r$, and in solvent with the generalized Born/surface area continuum method.[58] It was found that the energy difference between the different conformers decreased with increasing solvation treatment, and that the best correlation with experiment was with the continuum method. The partial charges on the ligand atoms were taken from AMBER, and those on the coordinated atoms and the iron were chosen to best fit the crystal structures while maintaining the formal ionic charge on the complex.

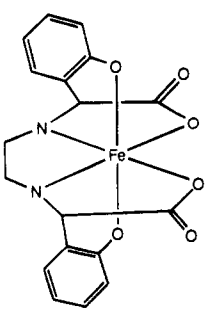

Figure 16. *S,S* rac conformer of Fe^{III}EHPG which is used as a transferrin model.

iv. Photosystem II

On the basis of spectroscopic measurements, a di-μ-oxo manganese dimer has been proposed as the active site for the oxygen evolving center in plant photosystem II and in manganese catalase. In order to computationally design a model system which would adopt specific structures e.g. a LMn_4O_4 cubane cluster, we modified the MM2* force field[51] for high-valent di-μ-oxo manganese dimer.[141] The force field was parameterized systematically. In the initial steps, monomeric manganese(III) and manganese(IV) complexes were used to determine ideal bond lengths and angles for an unhindered manganese(III) or manganese(IV) center, respectively. These were further refined to include the effects due to dimerization, and in the case of manganese(III), the Jahn–Teller distortions. We modeled the Jahn–Teller distortions by applying different ideal lengths for axial and equatorial metal–ligand bonds. Finally, the parameters described above were combined and further refined by modeling crystal structures of Mn^{III}–Mn^{III}, Mn^{IV}–Mn^{IV} and Mn^{III}–Mn^{IV} di-μ-oxo dimers. Due to the fact that these dimers are found with trapped valences, including distinguishable Jahn–Teller distorted Mn(III) and normal Mn(IV), we successfully minimized mixed-valence dimers by combining the Mn(III) and Mn(IV) parameters.

H. Metalloporphyrins and Related Complexes

MM calculations have often been used to analyze porphyrinoid complexes. One of the reasons for this is that the metal is usually coordinatively saturated and embedded in the ring system, thus the electrostatic effects are less important than they are in metalloproteins and they can be modeled in the same manner as inorganic molecular mechanics. A further simplification in the MM analysis of porphyrins is that the porphinato ligand binds the metal ion through its four nitrogen donors and the ideal N–M–N angles are 90° and 180° in square-planar and octahedral geometries (Figure 17).

However, the conjugation of the π systems in porphyrinoid complexes complicates the MM analysis of tetrapyrroles because despite the conjugation they are surprisingly flexible and can undergo a number of nonplanar deformations, such as ruffling and saddling[142] (Figure 18).

A valid force field should reproduce these geometric features. A calculated structure should have the same degree of pyrrole tilting and have the same torsional angles as the crystal structure, and it should be able to predict the direction and the extent of the metal displacement from the tetraaza plane.

Molecular dynamics simulations have been used to study the kinetics of dioxygen escape from the heme pocket of sperm whale myoglobin.[143] The AMBER united atom force field was used together with parameters derived from a vibrational analysis of metalloporphyrins.

A large number of porphyrin model compounds have been synthesized in order to model oxygen binding to heme. The majority of these models have

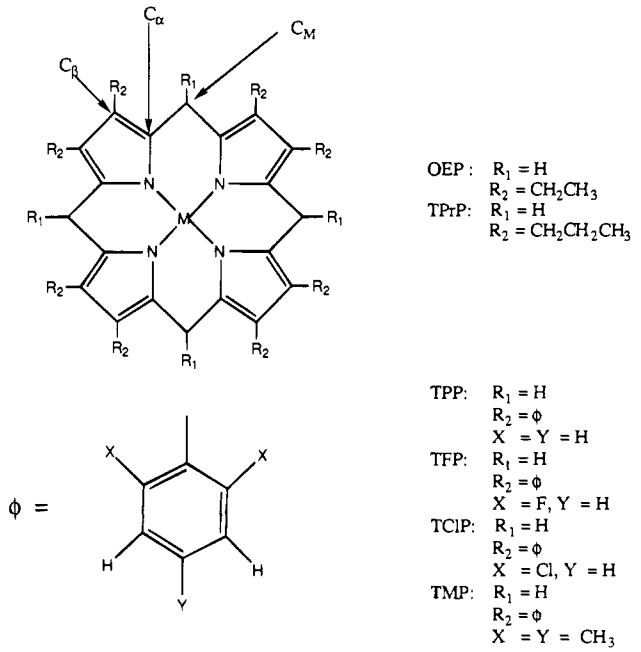

Figure 17. Commonly occurring porphyrinoid complexes and their abbreviations.

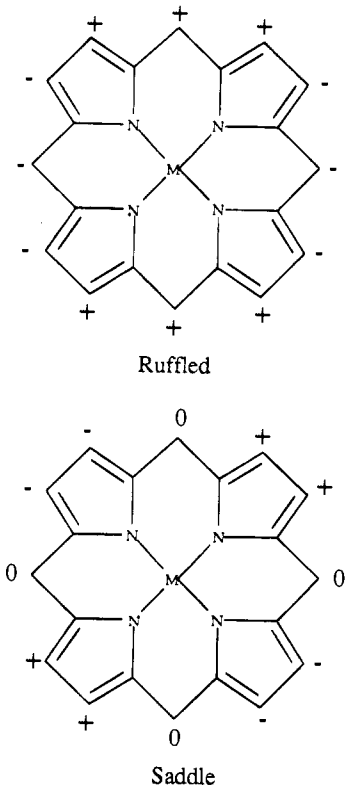

Figure 18. The two most common nonplanar distortions of tetrapyrroles. The "+" refers to carbons above the tetrazaplane, the "−", to carbons below the tetrazaplane, and 0, to carbons in the plane.

a ligand mimicking the proximal histidine, as well as cyclophanes, straps, pockets, pickets, caps, or baskets on the distal side of the tetrapyrrole. Kollman has modified his AMBER force field in order to investigate the relative binding affinities of oxygen and carbon monoxide to these models.[144,145] The parameters were modified by simulating the conformations of four heme complexes whose crystal structures were known and by calculating the partial charges on all atoms. The quality of the fit between the calculated and the known structure was judged on the basis of six criteria, these included factors such as the direction and extent of the iron atom displacement from the tetrapyrrole plane, and macrocylic hole size. The authors used molecular dynamics/free energy perturbations to study the origin of the preference for oxygen binding over carbon monoxide binding in four iron(II) porphyrin systems. By mutating CO into O_2 in the different models they were able to determine the role of steric and electrostatic effects in regulating these affinities. Solvent effects were ignored in these calculations because the O_2/CO binding site is well protected and because the calculations focused on the relative binding energy, which means that the solvent effects of the ligands should cancel. The force field was very effective at simulating the geometric properties, such as the extent of the displacement of the iron ion from the N_4 plane and the pyrrole tilting. The free-energy perturbations were successful in three of the four cases, in the fourth case it was assumed that solvent effects away from the binding site were responsible for its failure. For picket fence hemes, it was found that the oxygen preference is mainly due to electrostatic interactions, while in some other hemes the steric effects, due to the difference between the Fe−O−O angle of about 130° and the Fe−C−O angle of 180°, account for the binding differences.

Hancock published his molecular mechanical analysis on the role of steric hindrance in discriminating between the binding of dioxygen and carbon monoxide[146a] at the same time as Kollman's. The calculations were able to mimic the extent of ruffling in P(V), Ni(II), Fe(II), Zn(II), and Pb(II). Because the energies of the porphyrins coordinated to oxygen and those coordinated to carbon monoxide could not be compared directly, the authors compared the energies of the capped porphyrins after energy minimization and removal of the coordinated oxygen and carbon monoxide. It was found that steric effects have a considerable effect in determining the preferential binding of oxygen vs carbon monoxide.

A thorough full paper investigating ruffling in porphyrins by Hancock and Marques[42] followed the communication described above. They used standard MM2(87) parameters for all the interactions not involving the metal ion and retained the SCF π-MO calculations for all the delocalized π electrons. The parameters for the interactions involving the metal were determined by structure-based optimization of tetraphenylporphyrin complexes of P(V), Fe(II), an octaethylporphyrin complex of Ni(II), and a tetra-*n*-propylporphyrin lead(II) complex. No charges were used. The field was used to determine how the conformation of the porphyrinoid ligand is effected by the size of the metal, by the coordination of planar ligands like imidazole and by phenyl orientation. They found that the degree of S_4 ruffling of the porphyrin core is determined by the $M-N_{por}$ bond length and that by varying it they can mimic the ruffling as it is found with intermediately sized metals, such as Fe(II), Zn(II), and low- and high-spin Ni(II). In order to model the ruffling found in the small P(V), the torsions involving the P ion had to

be modified, and to model the large Pb(II) ion the metal torsion angles and the ideal N−M−N angle had to be changed. No conformational searches were undertaken. However, it was found that the planar Zn(II) conformation was obtained no matter whether the severely ruffled P(V) or the domed Pb(II) structure was used as a starting point for minimization. The core size of the porphyrin ligand was established by systematically varying the $M-N_{por}$ bond length and keeping all the force constants unchanged.[60] It was found that the ideal M−N length in the porphyrin ligand is 2.035 Å, and increasing bond lengths result in higher bond deformation energies, while shorter bond lengths are mainly responsible for increased nonbonded interactions. The porphyrin core was shown to be much more flexible than expected, in fact a planar porphyrin can undergo a core expansion of 0.15 Å with an increase of only 1.3 kcal/mol. The large high-spin Fe(II) can therefore be accommodated in the porphyrin cavity and does not need to be extruded. The authors conclude that steric factors are not responsible for the extrusion of Fe(II) in hemoglobin. As shown in Figure 18, there are two common nonplanar deformations, saddling (sad) and ruffling (ruf).[142] Ruffling can be induced by shortening the $M-N_{imid}$ distance of two trans axial imidazoles, whose planes are perpendicular to each other, and bisect the cis N−M−N angle of the porphyrin. Monitoring the nonplanar deformations while systematically varying the phenyl dihedral angle reveals that saddling only occurs at phenyl dihedral angles of 55° and greater. Because porphyrins have been shown to be more flexible than previously thought, the authors argue that nonplanar deformations are an efficient method to reduce nonbonded interactions in highly substituted metalloporphyrins.

Recently the force field described above[42] was improved by replacing the MM2 SCF-π-MO procedures with a localized bond model.[146b] The force field was modified by varying the parameters on a trial and error basis and optimizing the rmsd's between the bond lengths, angles, and dihedral angles of the crystal and calculated structures of seven iron(III) tetramesitylporphyrin(TMP) complexes. The accuracy of the field was also determined by fitting 25 core atoms and axial ligand donor atoms of the crystal structure with those of the calculated structure using the "fit" function of Alchemy III. The field accurately reproduced the contraction in the $Fe-N_p$ bond length observed in low-spin ferric porphyrins when they change from a planar to a ruffled conformation and showed that the porphyrin conformation is dependent on the nature and orientation of the axial ligands. Using conformational mapping methods,[147] it was demonstrated that the steric bulk of the meso-aryl groups is responsible for the amount of saddle-shaped (sad) ruffling. Mesityl group−axial ligand nonbonded interactions were observed, and it was suggested that these interactions were important in determining the energy-minimum orientations of ligands and substituents.

The axial ligand orientation in porphyrin complexes is interesting and has drawn considerable attention. In cytochrome b_5 and in three of the four cytochrome c_3 hemes the opposing imidazole rings are

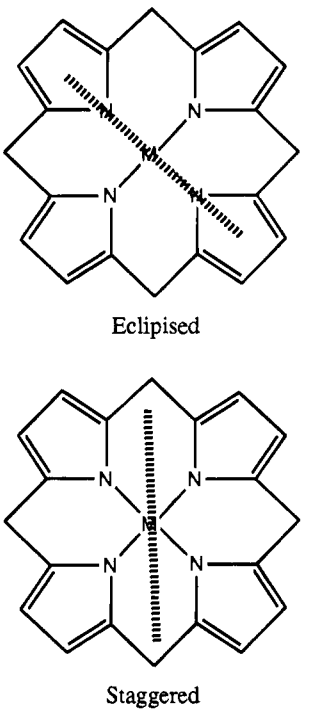

Figure 19. Ligand orientations in porphyrinoid complexes.

nearly parallel with each other, while in the remaining cytochrome c_3 heme the imidazole planes are nearly perpendicular. Hancock's MM2 parameters[42] were used to investigate the axial ligand orientations of iron(III) porphyrinates.[148] The energy profile that was obtained when both the axially coordinated pyridine rings in the bis-pyridine complexes of Fe^{III}-porphine, Fe^{III}TPP, and Fe^{III}TMP were rotated was essentially the same for all three complexes. Showing that the phenyl rings of iron^{III}TPP do not contribute to the rotational barrier of the two axial ligands. When comparing the calculated structures of the $[Fe(TPP)(Py)_2]^+$ and $[Fe(TMP)(4\text{-}NMe_2Py)_2]^+$ with their crystal structures, it was found that the calculated structures did not predict the correct amount of ruffling. It was suggested that this was due to additional electronic effects that favor ruffling and which are not included in the MM calculations. However, this effect might also be due to the fact that the authors used the MM2 parameters reported by Hancock[42] in the MM2* mode of MacroModel.[51] MM2* differs from MM2 in that it incorporates conjugation effects in the torsional, angular, and bond terms, while MM2 uses SCF-MO to calculate these effects. Therefore, Hancock's MM2 parameters will not be reliable when used in MacroModel, especially with respect to the degree of ruffling.

A NMR and MM analysis[149] of sterically hindered cobalt(III) porphyrins ligated to pyridine, 1-methylimidazole, 4-methylpiperidine, and isoquinoline, concluded that the planar ligands pyridine, 1-methylimidazole, and isoquinoline complex TPP and TFP in a staggered orientation, while TClP and TMP complex the ligands in an eclipsed conformation, Figures 17 and 19.

Ring current shifts of nuclei around and within the porphyrin core were calculated on the basis of the MM-minimized structures, they compared well with

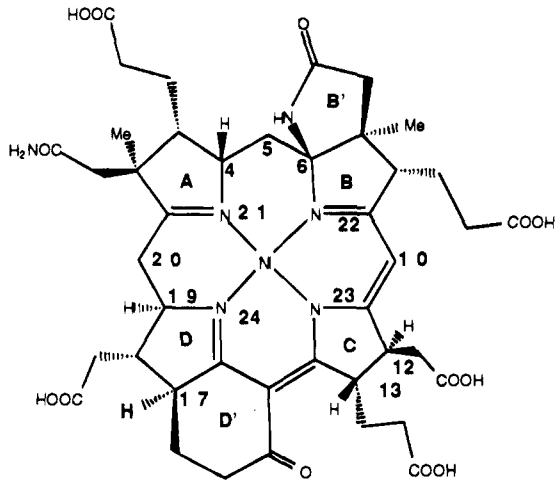

Figure 20. Structure of coenzyme F430.

the experimentally observed shifts. The MM calculations were done with the MODELS program[150] with partial charges that were determined using the CHARGE3 program.[151]

The CHARMm force field was used to investigate epoxidation by iron–oxo porphyrins[152] and a water-soluble closely interspaced cofacial zinc porphyrin dimer.[153] Calculational details are sparse and the MM calculations were used primarily for visualizing purposes.

Parameters to model 4- and 5-coordinated iron(II) porphyrin complexes, with the consistent valence force field (CVFF),[154] were generated from the crystal structure of a iron(II) prophyrin imidazole complex.[155] To test the force field two 4-coordinate and two 5-coordinate iron(II) porphyrinato complexes were modeled and compared with the crystal structure. The authors developed the parameters in order to compare the binding properties of a number of hypothetical polypeptide chelating arms with imidazole end groups to iron. The complexes were subjected to a MD conformational search with the imidazole uncoordinated and coordinated to the iron. The energies for the 4- and 5-coordinated forms were compared, and in all the cases examined, coordination by the imidazole ligand was favored.

It has been suggested that reducing the porphyrin ligand should result in a more flexible ligand.[156] This hypothesis was investigated by ligand binding and MM studies.[157] The binding constants for a series of six sterically hindered imidazoles with ZnTPP, Zn(2,3-dihydroTPP) and Zn(2,3,7,8-tetrahydroTPP) were determined. If the porphyrins become more flexible upon reduction one would expect the more reduced macrocycles to bind the more sterically hindered imidazoles better. However, only small differences in K_{eq} were measured with different porphyrinoid ligands. Using MMP2[158,159] parameters, qualitative agreement with the experimental binding constants was obtained and it was concluded that hydroporphyrins containing small metal ions are ruffled but rigid.

The changes that occur in the porphyrin core size and in its flexibility upon reduction of the porphyrin, and the implications of these changes on coenzyme F430 (Figure 20) were investigated using the same force field.[160]

All the modified and additional parameters were presented; however, details of their derivation were not presented. Interestingly the N–Ni–N bond angle and the C–C–N–Ni torsional angles were given force constants of zero. No mention was made of how 4-coordinate complexes were kept from adopting a tetrahedral geometry. The parameters were tested by comparing the calculated and the crystal structures of 10 nickel(II) (hydro)porphyrinoid complexes. The core size determinations were undertaken by systematically varying the ideal Ni–N distance, while retaining the standard Ni–N force constant. In order to remove it from all the atom–atom repulsions, the nickel ion was given a van der Waals radius of zero for all core size determinations. The core size determinations were done without considering any substituents on the core and without any conformational searches between steps. They indicated that the macrocyclic core size increases when the reduction occurs at the β-pyrrole positions (chlorin, isobacteriochlorin, pyrrocorphin), and decreases when the reduction occurs at the methine positions (hexahydroporphyrin, coenzyme F430). Furthermore, in contrast to the previous calculations[157] which indicated that reduction at the β-pyrrole positions did not result in increased flexibility, these calculations show that reduction at the methine positions increase the flexibility. It would be interesting to see what effect the cyclohexanone and lactone rings, which were ignored in the core size determinations, have on the flexibility of F430.

We have used a modified MM2* force field to investigate all the coordination geometries available to nickel in coenzyme F430.[43] The nickel(II) high- and low-spin parameters were based on those reported by Hancock[161,162] and were modified by simulating porphyrinoid crystal structures. The parameters were tested by comparing the calculated and solid-state structures of planar and highly ruffled porphyrinoid complexes that were not used in the parameter modification. By ignoring the energy due to axial ligation we were able to compare 4- and 5-coordinate nickel geometries and concluded that the hydroporphyrinoid core of coenzyme F430 was sufficiently flexible to accepted a trigonal bipyramidal (TBP) geometry around the nickel ion. Saunder's random kick search method[49] was used to find all low-energy minima, as this proved to be the most efficient search method for coenzyme F430. In order to determine the best fit Ni–N length the Ni–N distance was systematically varied while keeping all parameters constant, including the Ni–N force constant which was held at a value halfway between that for nickel(II) high and low spin. This revealed that coenzyme F430 has a larger ideal Ni–N distance in the TBP geometry than in the square planar (SP) geometry. The ideal Ni–N distance of 2.05 Å for F430 ligating the metal ion in a SP geometry is 0.05 Å larger than that reported in the previous study. The possible reasons for this are that the previous study only examined the hydroporphyrinoid core of F430 without the lactone and cyclohexanone rings and that the metal van der Waals interactions were not removed in our study.

Coenzyme F430 is thermally unstable and it epimerizes to 13-epi F430 and then to 12,13-diepi F430. The crystal structure of the 12,13-diepi F430M derivative was solved after the paper described above[43] was published. The MM2* force field used in the paper correctly and accurately modeled the conformation, bond lengths, and bond angles of the 12,13-diepimer.[163] We were also able to show that while the 13-epimer and 12,13-diepimer of F430 have a ruffled conformation, the native form has a saddle-shaped macrocycle. The flexibility, around the N21–Ni–N23 axis, of both the native form and 12,13-diepi F430M was investigated by systematically varying the ideal N–Ni–N angle while maintaining the standard force constant. A conformational search was required every 10°, as both complexes underwent conformational changes upon bending. Our initial finding[43] that coenzyme F430 might adopt a trigonal bipyramidal geometry around the nickel *in vivo* was reconfirmed.

Cytochrome P450 metabolizes the antiepileptic agent, valproic acid. The stereospecificity and product distribution of the hydroxylated metabolites of valproic acid were predicted on the basis of MM and molecular dynamics calculations.[164] The crystal structure of adamantanone-bound $P450_{cam}$ was used as the starting point for the graphic construction of valproic acid-P450 complexes, which were minimized using AMBER. The charges were determined by INDO/S calculations, and although the iron parameters are presented, their derivation is not described. Only the "binding site" was minimized, it consisted of 87 noncontiguous amino acids, and therefore the backbone was constrained, while all side-chain, porphyrin, and substrate molecules were allowed to move freely.

Similar methods were subsequently used by the same group to model the epoxidation of *cis*-β-methylstyrene, *trans*-β-methylstyrene, and styrene by cytochrome $P450_{cam}$.[165,166] A good agreement was obtained between the molecular dynamically predicted enantiomeric excess and that observed experimentally. The experimentally observed trend was also predicted in a study of cytochrome $P450_{cam}$ oxidation of thioanisole and *p*-methylthioanisole.[167] The same methods and field were also used to examine the role threonine 252 plays in the oxygen activation of cytochrome $P450_{cam}$.[168]

In a series of papers Shelnutt has used MM to correlate structural properties of planar and nonplanar porphyrins with their spectroscopic properties (mainly Raman frequencies). The parameters were based on the DREIDING field and were derived from a previously published normal coordinate analysis of nickel(II) OEP[169-171] and a crystal structure of NiOEP.[172] Electrostatic energy terms had little effect on the calculated structures and partial charges were excluded in the first generation of the force field.[36] The degree of nonplanarity, core size, and C_α–N–C_α angle were correlated with Raman frequencies.[36] There are two modes of ruffling, they were measured by determining (1) the degree of pyrrole twisting (ruf), defined by the dihedral angle between the planes of opposite pyrrole rings, and (2) the degree of pyrrole tilting (sad), defined by the angle between opposing pyrroles (Figure 18). The total strain energy was shown to be related to the nonplanarity of the macrocycle and the size of the β-pyrrole substituents. The field reproduces the basic conformation of nickel(II) octaalkyl(aryl)tetraphenylporphyrins, but slightly overestimates the amount pyrrole twisting.

The same field was used to analyze the conformations of dodecaphenylporphyrin and dodecaalkylporphyrins. In order to avoid local minima, planar, ruffled, and saddle conformations were used as starting points for minimization, and the initial energy minimum structures were subjected to molecular dynamics before minimizing again.[173] One of the structures investigated was highly ruffled, while another was in a saddle conformation, both nonplanar distortions were correctly predicted by MM calculations.

In order to establish the effect of metal size on the degree of nonplanar distortions in porphyrins the above-mentioned force field was expanded to include Co(II), Cu(II), Zn(II), Co(III), and Fe(III).[37] The conformations of the complexes of these metals with octaethylporphyrins (OEP), tetraphenylporphyrins (TPP), and the highly distorted octaethyltetraphenylporphyrins (OETPP) were calculated and when possible they were compared with the crystallographically determined structures. New equilibrium M–N distances, homonuclear nonbonded separations, and atomic masses were added for the unparameterized metals. The force constants, the depth of the Lennard-Jones 12-6 potential well and the parameters for the torsions, inversions and angle deformations were all left at the values used for nickel(II). The calculations modeled the solid-state structures with RMS out-of-plane deviations of less than 0.1 Å, slightly larger deviations were found for porphyrins with axial ligands. In both the crystal structures and in the calculated structures it was found that the C_α–N–C_α and C_α–C_m–C_α angles open as the core size increases due to the addition of larger metals. The increase in the bond length of the C_α–C_m and C_β–C_β bonds, as well as the flattening of the macrocycle that is caused by larger metals was accurately modeled. The conformations determined by the MM calculations described above were used in INDO/CI molecular orbital calculations and successfully predicted the trends in the π–π^* transition energies for nickel porphyrins. The authors found that the practice of simplifying the MO calculations by using planar porphyrin structures and ignoring the substituents leads to incorrect results, and that the combination of MM and the INDO/CI method is very effective at predicting optical spectra.

X-ray crystal structures of both planar and nonplanar conformations of nickel(II) octaethylporphyrin have been found, and in noncoordinating solvents they have been shown to coexist in equilibrium. The amount of steric interactions that are required to influence the equilibrium and the effect of metal-induced core contraction on the planar/nonplanar equilibrium was investigated[174] using the field described in the previous paragraph. It was MM and experimentally found that substituting a single NO_2 group at one of the methine-bridge carbons (Figure 21) shifts the equilibrium to the nonplanar conformation.

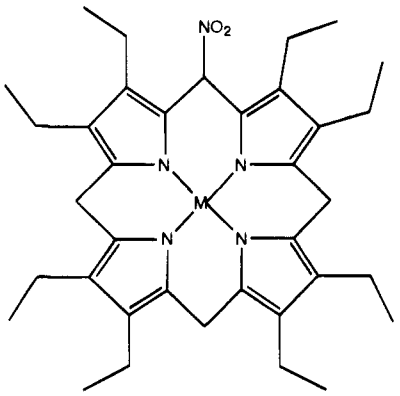

Figure 21. Structure of a nitrooctaethylporphyrin complex.

This conformational change is accompanied by a slight core expansion which relieves the steric repulsions between the nitro group and the neighboring ethyl side chains of the porphyrin. The calculated nitrooctaethylporphyrin conformation agrees well with that found in the crystal structure. Nonplanar distortions are promoted by core contractions induced by small metals such as Ni and Co, but not for larger ones like Cu and Zn. The authors conclude that the influence of the protein matrix on the porphyrin conformation in porphyrin-containing proteins can only be modeled by severe steric crowding, such as is observed in dodecasubstituted porphyrins.

In earlier modeling studies Shelnutt and co-workers had predicted that (tetraphenyltetrapropanoporphinato)nickel(II) should be planar;[36,175] however, due to its poor solubility no crystals were obtained of the compound and these predictions could not be verified. Therefore nickel(II) and copper(II) complexes of tetrakis(3,4,5-trimethoxyphenyl)tetrapropanoporphyrin, which were predicted to be planar by MM calculations, were synthesized and crystallized.[176] The solid-state structures showed that the copper(II) complex was planar, as predicted, but that the nickel(II) complex adopted a slightly nonplanar conformation. Two possible causes, suggested by the authors for the failure of their force field to account for the slight nonplanar deformation, were that the field does not take into account crystal packing forces and that the molecular dynamics search could not traverse the energy barrier between different planar and nonplanar conformations.

The effect of changing the metal from Ni(II) to Co(II) and Cu(II), on the nonplanar distortions of tetracyclohexenyltetraphenylporphyrin was modeled with MM calculations.[177] In the same paper the increasing nonplanarity that results when the size of the alkyl ring at the β carbon on the pyrrole rings is increased from tetracyclopentenyltetraphenylporphyrin to tetracyclohexenyltetraphenylporphyrin and tetracycloheptenyltetraphenylporphyrin was reproduced with MM for nickel(II) complexes. The calculated structures and parameters (e.g. core size, the $C_\alpha-N-C_\alpha$ angle) were used to correlate the nonplanarity of the tetrapyrroles with Raman frequencies. The parameters described above[37] were used with partial atomic charges taken from the DREIDING force field.[32]

A series of nickel(II) *meso*-nitrooctaethylporphyrins have been investigated by MM, resonance Raman, NMR, and UV–visible spectroscopy.[178] The Shelnutt force field[36,37] was further modified by adding electrostatic terms and by changing the van der Waals energy term for hydrogen atoms from a Lennard-Jones 6-12 to an exponential (r^{-6}) term. These changes did not have a great effect on the geometries of the minimized structures; however, it improved the relative energies of the low-energy conformers. It was found that the root-mean-square out-of-plane distance is a good measure of the degree of the nonplanar distortion of the tetrapyrrole, regardless of whether it is a saddle or a ruffled distortion, and that it increases with each additional meso-nitro substitution. As seen with the octaalkyltetraphenyl porphyrins[36,37] the calculated Ni–N distances and the core size decrease with increasing nonplanarity. For tetranitrooctaethylporphyrin six different conformers with varying degrees of ruffling were found within 2.0 kcal/mol of each other. Although the nonplanarity, as measured by the root-mean-square out-of-plane distance, of all the conformers was similar, the amount of saddle vs ruffling distortion differed significantly and was dependent on the ethyl orientations. While NMR results confirm the existence of multiple low-energy conformers, they are not observed in resonance Raman spectra. However, the degree of the nonplanar distortion predict by MM calculations matches that observed by Raman techniques.

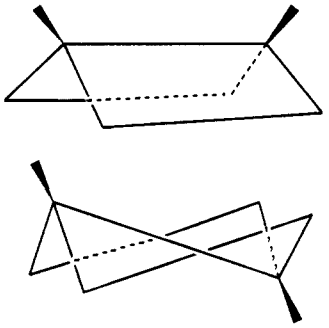

Figure 22. Syn (top) and anti (bottom) structures of decaalkylporphyrin. The wedges represent the alkyl substituents at positions 5 and 15.

Recently,[47] Shelnutt and co-workers have extended their study of the factors that induce nonplanar distortions in dodecasubstituted porphyrins to decasubstituted porphyrins, specifically the zinc(II), copper(II), and nickel(II) complexes of hexaethyltetramethylporphyrin. The charge equilibration method[46] was used to determine the partial charges. MM calculations reproduced the nonplanar distortions observed in the solid-state structures of the copper(II) and nickel(II) complexes. However, the MM simulation of the dodecasubstituted zinc(II) complexes were significantly better than the decasubstituted complexes (rms of 0.09 Å vs 0.15 Å). A number of low-energy zinc(II) conformers were found. They were all syn conformers (see Figure 22) which is in disagreement with a variable-temperature study that has proposed that the zinc(II) complex is a mixture of syn and anti conformations.[179]

The Shelnutt force field[36,37,178] has also been used to analyze the structure of a (μ-oxo)bis[(octaethylporphinato)iron(III)] dimer.[180] In order to model the dimer, new parameters were derived for the bridging

μ-oxo group. The calculations reproduced all the structural features of the dimer, including the unusual eclipsing of the two porphyrins which is observed in the solid-state structures. The two rings eclipse in order to interdigitate the substituent ethyl groups. When the dimer is minimized without the ethyl groups the N−Fe−Fe′−N′ dihedral angle increases from 16° to 31°.

MM methods have also been used to calculate the conformation of iron(III)[181] and gallium(III)[182] 2-hydroxy-5,10,15,20-tetraphenylporphyrin trimers. These complexes have been characterized by numerous spectroscopic methods. However, no crystals suitable for X-ray crystallography were obtained. Therefore, in order to get some idea of the structure of the trimer MM calculations were undertaken. The MM+ field in HyperChem was modified to incorporate iron(III) and gallium(III). The metals were not minimized and their positions were constrained in the porphyrin cavity. The constraints were based on average iron(III)− and gallium(III)−nitrogen bond distances, and on out-of-plane deformations found in solid-state structures. No mention of any attempts to test the validity of these modifications is made, nor were any conformational searches conducted.

VI. Concluding Remarks and Future Consideration

Molecular mechanical methods are remarkably accurate at modeling the solid-state geometries of small bioinorganic molecules. Although this is gratifying, it is not extremely useful. MM calculations are more impressive and useful when they are used to predict and design new structures and properties. Since most chemistry occurs in solution it is important to be able to model solvent effects. This is a computationally intensive procedure and approaches such as the GB/SA approximation are useful. However, they require an accurate knowledge of the charge distribution. An alternative method of finding the solution structure is to find all the low-energy conformations of a molecule and use them to simulate spectroscopic properties. By comparing the simulated and experimental spectral characteristics the conformations present in solution can be picked out. The most obvious spectroscopic properties to compare would be NOE distances, but EPR[183,184] and UV[185] have been used in inorganic MM simulations. The reasoning described above could be reversed to computationally design bioinorganic model systems with desired spectroscopic properties.[185]

I think MM simulations will become increasingly important in the rational design of biomimetic compounds. We are currently busy designing urease model systems. The mechanism and some EXAFS studies of urease have been used to generate some geometric constraints for the model e.g. metal−metal distance of 5.0−6.0 Å. These constraints have been incorporated in a Cambridge Database search, and the hits have been analyzed and modified by molecular mechanics and dynamics, in order to fulfill a set of urease model criteria that we have established.

While MM calculations accurately model the geometries of small bioinorganic molecules, the simulation of metalloproteins is more complex because good starting structures are needed as it is impossible to find the global minima with current conformational searching methods. Solid-state structures, such as the newly resolved structures of urease, hydrogenase[186] and nitrogenase[187,188] are a good starting point for such MM calculations.

VII. References

(1) 1. Andrews, D. H. *Phys. Rev.* **1930**, *36*, 544.
(2) Hill, T. L. *J. Chem. Phys.* **1946**, *14*, 465.
(3) Westheimer, F. H. *J. Chem. Phys.* **1946**, *14*, 733.
(4) Allinger, N. L. *Adv. Phys. Org. Chem.* **1976**, *13*, 1.
(5) Allinger, N. L. *J. Am. Chem. Soc.* **1977**, *99*, 8127.
(6) Allinger, N. L.; Yuh, Y. H.; Lii, J.-H. *J. Am. Chem. Soc.* **1989**, *111*, 8551.
(7) Nakamoto, K. *Infrared and Raman Spectra of Inorganic and Coordination Compounds*, 3rd ed.; Wiley: New York, 1978.
(8) Vedani, A.; Dunitz, J. D. *J. Am. Chem. Soc.* **1985**, *107*, 7653.
(9) Hoops, S. C.; Anderson, K. W.; Merz, K. M., Jr. *J. Am. Chem. Soc.* **1991**, *113*, 8260.
(10) Burkert, U.; Allinger, N. L. *Molecular Mechanics*; ACS Monograph, 177; American Chemical Society: Washington, DC, 1982.
(11) Mathieu, J.-P. *Ann. Phys.* **1944**, *19*, 335.
(12) Corey, E. J.; Bailar, J. C. *J. Am. Chem. Soc.* **1959**, *81*, 2620.
(13) Buckingham, D. A.; Marzilli, L. G.; Sargeson, A. M. *J. Am. Chem. Soc.* **1967**, *89*, 825.
(14) Gollogly, J. R.; Hawkins, C. *Inorg. Chem.* **1967**, *20*, 2395.
(15) Gollogly, J. R.; Hawkins, C. *Inorg. Chem.* **1969**, *8*, 1168.
(16) Gollogly, J. R.; Hawkins, C. *Inorg. Chem.* **1970**, *9*, 576.
(17) Gollogly, J. R.; Hawkins, C.; Beattie, J. K. *Inorg. Chem.* **1971**, *10*, 317.
(18) Gollogly, J. R.; Hawkins, C. *Inorg. Chem.* **1972**, *11*, 156.
(19) Hancock, R. D. *Acc. Chem. Res.* **1990**, *23*, 253.
(20) Comba, P. *Coord. Chem. Rev.* **1993**, *123*, 1.
(21) Hay, B. P. *Coord. Chem. Rev.* **1993**, *126*, 177.
(22) Brubaker, G. R.; Johnson, D. W. *Coord. Chem. Rev.* **1984**, *53*, 1.
(23) Comba, P. *Comments Inorg. Chem.* **1994**, *16*, 133.
(24) Comba, P.; Zimmer, M. *J. Chem. Educ.*, in press.
(25) Hancock, R. D. *Prog. Inorg. Chem.* **1989**, *37*, 187.
(26) Bosnich, B. *Chem. Soc. Rev.* **1994**, 387.
(27) Comba, P.; Hambley, T. W. *Molecular Modelling of Inorganic and Coordination Compounds*; VCH Publishers: Weinheim, in press.
(28) Allured, V. S.; Kelly, C. M.; Landis, C. R. *J. Am. Chem. Soc.* **1991**, *113*, 1.
(29) Weiner, P. K.; Kollman, P. A. *J. Comput. Chem.* **1981**, *2*, 287. Weiner, S. J.; Kollman, P. A.; Nguyen, D. T.; Case, D. A. *J. Comput. Chem.* **1986**, *7*, 230.
(30) Comba, P.; Hambley, T. W. A molecular mechanics program for coordination compounds adapted to HyperChem.
(31) Brooks, R.; Bruccoleri, R. E.; Olafson, B. D.; States, D. J.; Swaminathan, S.; Karplus, M. *J. Comput. Chem.* **1983**, *4*, 187.
(32) Mayo, S. L.; Olafson, B. D.; Goddard, W. A., III. *J. Phys. Chem.* **1990**, *94*, 8897.
(33) Lin, W.; Welsh, W. J.; Harris, W. R. *Inorg. Chem.* **1994**, *33*, 884.
(34) Charles, R.; Ganly-Cunningham, M.; Warren, R.; Zimmer, M. *J. Mol. Struct.* **1992**, *265*, 385.
(35) Rappe, A. K.: Colwell, K. S.; Casewit, C. J. *Inorg. Chem.* **1993**, *32*, 3438.
(36) Shelnutt, J. A.; Medforth, C. J.; Berber, M. D.; Barkigia, K. M.; Smith, K. M. *J. Am. Chem. Soc.* **1991**, *113*, 4077.
(37) Sparks, L. D.; Medforth, C. J.; Park, M.-S.; Chamberlain, J. R.; Ondrias, M. R.; Senge, M. O.; Smith, K. M.; Shelnutt, J. A. *J. Am. Chem. Soc.* **1993**, *115*, 581.
(38) Comba, P.; Zimmer, M. *Inorg. Chem.* **1994**, *33*, 5368.
(39) Drew, M. G. B.; Yates, P. C. *Pure Appl. Chem.* **1989**, *61*, 835.
(40) Canales, C.; Zimmer, M. *J. Mol. Struct.* **1991**, *245*, 341.
(41) Hambley, T. W.; Hawkins, C. J.; Palmer, J. A.; Snow, M. R. *Aust. J. Chem.* **1981**, 34, *45*.
(42) Munro, O.; Bradley, J. A.; Hancock, R. D.; Marques, H. M.; Marsicano, F.; Wade, P. W. *J. Am. Chem. Soc.* **1992**, *114*, 7218.
(43) Zimmer, M.; Crabtree, R. H. *J. Am. Chem. Soc.* **1990**, *112*, 1062.
(44) Pettit, B. M.; Karplus, M. *J. Am. Chem. Soc.* **1985**, *107*, 1166.
(45) Vedani, A.; Dobler, M.; Dunitz, J. D. *J. Comput. Chem.* **1986**, *7*, 701.
(46) Rappe, A. K.; Goddard, W. A. *J. Phys. Chem.* **1991**, *95*, 3358.
(47) Medforth, C. J.; Senge, M. O.; Forsyth, T. P.; Hobbs, J. D.; Shelnutt, J. A.; Smith, K. M. *Inorg. Chem.* **1994**, *33*, 3865.
(48) Saunders, M.; Houk, K. N.; Wu, Y.-D.; Still, W. C.; Lipton, M.; Chang, G.; Guida, W. C. *J. Am. Chem. Soc.* **1990**, *112*, 1419.
(49) Saunders, M. *J. Am. Chem. Soc.* **1987**, *109*, 3150.
(50) Chang, G.; Guida, W. C.; Still, W. C. *J. Am. Chem. Soc.* **1989**, *11*, 4379.
(51) Mohamdi, F.; Richards, N. G. J.; Guida, W. C.; Liskamp, R.; Lipton, M.; Caufield, C.; Chang, G.; Hendrickson, T.; Still, W. C. *J. Comput. Chem.* **1990**, *11*, 440.

(52) Schweizer, W. B. *Structure Correlation*; VCH Publishers: New York, 1994; Vol. 1.
(53) Van Gunsteren, W. F. First European Conference on Computational Chemistry, Nancy, France, May, 1994.
(54) McDonald, D. Q; Still, W. C. *J. Am. Chem. Soc.* **1994**, *116*, 11550.
(55) Kaitner, B.; Paulic, N.; Raos, N. *J. Coord. Chem.* **1991**, *24*, 291.
(56) Zimmer, M. *J. Biomol. Struc. Dyn.* **1993**, *11*, 203.
(57) Tueting, J. L.; Spence, K. L.; Zimmer, M. *J. Chem. Soc., Dalton Trans.* **1994**, 551.
(58) Still, W. C.; Tempczyk, A.; Hawley, R. C.; Hendrickson, T. *J. Am. Chem. Soc.* **1990**, *112*, 6127.
(59) Drew, M. G. B.; Hollis, S.; Yates, P. C. *J. Chem. Soc. Dalton Trans.* **1985**, 654.
(60) Hancock, R. D. *J. Chem. Soc. Dalton Trans.* **1986**, 2505.
(61) Thomas, M. W.; Emerson, D. *J. Mol. Struct.* **1973**, *16*, 473.
(62) Van de Graaf, F.; Baas, J. M. A. *Recl. Trav. Chim. Pays-Bas* **1980**, *99*, 327.
(63) Hambley, T. W. *J. Comput. Chem.* **1987**, *8*, 651.
(64) Buckingham, D. A.; Maxwell, I. E.; Sargeson, A. M.; Snow, M. R. *J. Am. Chem. Soc.* **1970**, *92*, 3617.
(65) Buckingham, D. A.; Cresswell, P. J.; Dellaca, R. J.; Dwyer, M.; Gainsford, G. J.; Marzilli, L. G.; Maxwell, I. E.; Robinson, W. T.; Sargeson, A. M.; Turnbull, K. R. *J. Am. Chem. Soc.* **1974**, *96*, 1713.
(66) Buckingham, D. A.; Dwyer, M.; Gainsford, G. J.; Janson, V.; Ho, L.; Marzilli, L. G.; Robinson, W. T.; Sargeson, A. M.; Turnbull, K. R. *Inorg. Chem.* **1975**, *14*, 1939.
(67) Anderson, B. F.; Bell, J. D.; Buckingham, D. A.; Creswell, P. J.; Gainsford, G. J.; Marzilli, L. G.; Robertson, G. B.; Sargeson, A. M. *Inorg. Chem.* **1977**, *16*, 3233.
(68) Hambley, T. W. *Acta Crystallogr.* **1988**, *B44*, 601.
(69) Brubaker, G. R.; Massura, J. G. *J. Coord. Chem.* **1974**, *3*, 251.
(70) Yates, P. C. *J. Mol. Struct. (THEOCHEM)* **1993**, *281*, 275.
(71) Juranic, N.; Likic, V.; Kostic, N.; Macura, S. *Inorg. Chem.* **1995**, *34*, 938.
(72) Ferraro, J. R. *Low-Frequency Vibrations of Inorganic and Coordination Compounds*; Plenum Press: New York, 1971.
(73) Raos, N.; Simeon, V. *Croat. Chem. Acta* **1985**, *58*, 127.
(74) Raos, N.; Simeon, V. *Croat. Chem. Acta* **1983**, *56*, 79.
(75) Kainter, B.; Kamenar, B.; Paulic, N.; Raos, N.; Simeon, V. *J. Coord. Chem.* **1987**, *15*, 373.
(76) Sabolovic, J.; Raos, N.; Rasmussen, K. *Croat. Chem. Acta* **1989**, *62*, 495.
(77) Raos, N.; Simeon, V. *Croat. Chem. Acta* **1984**, *57*, 1217.
(78) Kamenar, B.; Penavic, M.; Skoric, A.; Paulic, N.; Raos, N.; Simeon, V. J. *Coord. Chem.* **1988**, *17*, 85.
(79) Kaitner, B.; Ferguson, G.; Paulic, N.; Raos, N. *J. Coord. Chem.* **1993**, *29*, 247.
(80) Raos, N.; Niketic, S. R.; Simeon, V. *J. Inorg. Biochem.* **1982**, *16*, 1.
(81) Sabolovic, J.; Raos, N.; Rasmussen, K. *Polyhedron* **1991**, *10*, 2079.
(82) Sabolovic, J.; Raos, N. *Polyhedron* **1990**, *9*, 1277.
(83) Sabolovic, J.; Raos, N. *Polyhedron* **1990**, *9*, 2419.
(84) Kozelka, J. *Met. Ions Biol. Systems*, in press.
(85) Mustafi, D.; Telser, J.; Makinen, M. *J. Am. Chem. Soc.* **1992**, *114*, 6219.
(86) Dayringer, H. E.; Tramontano, A.; Sprang, S. R.; Fletterick, R. J. *J. Mol. Graphics* **1986**, *4*, 82.
(87) Tripos Associates, Inc., 1600 S. Hanley Road, St. Louis, MO 63144.
(88) Cini, R.; Giorgi, G.; Lashi, F.; Rossi, C.; Marzilli, L. G. *J. Biomol. Struct. Dyn.* **1990**, *7*, 859.
(89) Jolly, W. L.; Perry, W. B. *Inorg. Chem.* **1974**, *13*, 1211.
(90) Sardesai, N. Y.; Zimmerman, K.; Barton, J. K. *J. Am. Chem. Soc.* **1994**, *116*, 7502.
(91) Collins, J. G.; Shields, T. P.; Barton, J. K. *J. Am. Chem. Soc.* **1994**, *116*, 9840.
(92) Haworth, I. S.; Elcock, A. H.; Freeman, J.; Rodger, A.; Richards, W. G. *J. Biol. Mol. Struct. Dyn.* **1991**, *9*, 23.
(93) Mejzlik, P. *J. Biomol. Struct. Dyn.* **1994**, *12*, 327.
(94) Frisch, M. J.; Head-Gordon, H.; Trucks, G. W., Gausian, Inc. Pittsburgh, PA, 1990.
(95) Stevens, W. J.; Krauss, M.; Basch, H.; Jasien, P. G. *Can. J. Chem.* **1992**, *70*, 612.
(96) Araki, K.; Tajima, H. *J. Inorg. Biochem.* **1993**, *52*, 89.
(97) Bunel, S.; Ibarra, C.; Moraga, E.; Blasko, A.; Bunton, C. *Carbohyd. Res.* **1993**, *244*, 1.
(98) Comba, P.; Jakob, H.; Nuber, B.; Keppler, B. K. *Inorg. Chem.* **1994**, *33*, 3396.
(99) Stubbe, J.; Kozarich, J. W. *Chem. Rev.* **1987**, *87*, 1107.
(100) Hecht, S. M. *Acc. Chem. Res.* **1986**, *19*, 383.
(101) Sugiura, Y.; Takita, T.; Umezawa, H. *Met. Ions Biol. Syst.* **1985**, *19*, 81.
(102) Carter, B. J.; Murty, V. S.; Reddy, K. S.; Wang, S.-N.; Hecht, S. M. *J. Biol. Chem.* **1990**, *265*, 4193.
(103) Iitaka, Y.; Nakamura, H.; Nakatani, T.; Muraoka, Y.; Fujii, A.; Takita, T.; Umezawa, H. *J. Antibiot.* **1978**, *31*, 1070.
(104) Takita, T.; Muraoka, Y.; Nakatani, T.; Fuji, A.; Iitaka, Y.; Umezawa, H. *J. Antibiot.* **1978**, *31*, 1073.
(105) Akkerman, M. A. J.; Neijman, E. W. J. F.; Wijmenga, S. S.; Hilbers, C. W.; Bermel, W. *J. Am. Chem. Soc.* **1990**, *112*, 7462.
(106) Akkerman, M. A. J.; Haasnoot, C. A. G.; Pandit, U. K.; Hilbers, C. W. *Magn. Reson. Chem.* **1988**, *26*, 793.
(107) Tueting, J. L; Spence, K. L.; Zimmer, M. *J. Chem. Soc., Dalton Trans.* **1994**, 551.
(108) Wu, Y.-D.; Houk, K. N.; Valentine, J. S.; Nam, W. *Inorg. Chem.* **1992**, *31*, 718.
(109) Guajardo, R. J.; Tan, J. D.; Mascharak, P. K. *Inorg. Chem.* **1994**, *33*, 2838.
(110) Hambley, T. W. *Comments Inorg. Chem.* **1992**, *14*, 1.
(111) Kozelka, J.; Archer, S.; Petsko, G.; Lippard, S.; Quigley, G. J. *Biopolymers* **1987**, *26*, 1245.
(112) Kozelka, J.; Chottard, J. C. *Biophys. Chem.* **1990**, 35, 165.
(113) Herman, F.; Kozelka, J.; Stoven, V.; Guittet, E.; Girault, J.-P.; Huynh-Dinh, T.; Igolen, J.; Lallemand, J.-Y.; Chottard, J.-C. *Eur. J. Chem.* **1990**, *194*, 119.
(114) Reily, M. D.; Hambley, T. W.; Marzilli, L. G. *J. Am. Chem. Soc.* **1988**, *110*, 2999.
(115) Miller, K.; McCarthy, S. L.; Krauss, M. *J. Med. Chem.* **1990**, *33*, 1043.
(116) McCarthy, S. L.; Hinde, R. J.; Miller, K. J.; Anderson, J. S.; Basch, H.; Krauss, M. *Biopolymers* **1990**, *29*, 785.
(117) McCarthy, S. L.; Hinde, R. J.; Miller, K. J.; Anderson, J. S.; Basch, H.; Krauss, M. *Biopolymers* **1990**, *29*, 823.
(118) Hambley, T. W. *Inorg. Chem.* **1988**, *27*, 1073.
(119) Hambley, T. W. *J. Chem. Soc., Chem. Commun.* **1988**, 221.
(120) Hambley, T. *Inorg. Chem.* **1991**, *30*, 937.
(121) Kozelka, J.; Savinelli, R.; Berthier, G.; Flament, J.-P.; Lavery, R. *J. Comput. Chem.* **1993**, *14*, 45.
(122) Sip, M.; Schwartz, A.; Vovelle, F.; Ptak, M.; Leng, M. *Biochemistry* **1992**, *31*, 2508.
(123) Nikolov, G. S.; Trendafilova, N.; Schoenenberger, H.; Gust, R.; Kritzenberger, J.; Yersin, H. *Inorg. Chem. Acta* **1994**, *217*, 159.
(124) Vickery, K.; Bonin, A. M.; Fenton, R. R.; O'Mara, S.; Russel, P. J.; Webster, L. K.; Hambley, T. W. *J. Med. Chem.* **1993**, *36*, 3663.
(125) (a) van Garderen, C. J.; van Houte, L. P. A. *Eur. J. Biochem.* **1994**, *225*, 1169. (b) Yao, S.; Plastaras, J. P.; Marzilli, L. *Inorg. Chem.* **1994**, *33*, 6061. (c) Veal, J. M.; Wilson, D. W. *J. Biomol. Struct. Dyn.* **1991**, *8*, 1119.
(126) Bouraoui, A.; Fathallah, M.; Blaive, B.; Gallo, R.; M'Henni, F. *J. Chem. Soc., Perkin Trans.* **1990**, *2*, 1211.
(127) Bouraoui, A.; Fathallah, M.; M'Henni, F.; Blaive, B.; Gallo, R. Modelling of Molecular Structures and Properties. Proc. of Int. Meeting, Nancy, France, 1989.
(128) Zinelabidine, A.; Bouraoui, A.; M'Henni, F.; Blaive, B.; Gallo, R. *J. Mol. Struct.* **1993**, *286*, 267.
(129) Hansen, L.; Cini, R.; Taylor, A., Jr.; Marzill, L. G. *Inorg. Chem.* **1992**, *31*, 2801.
(130) Marzilli, L. G.; Banaszczyk, M. G.; Hansen, L.; Kuklenyik, Z.; Cini, R. ; Taylor, A., Jr. *Inorg. Chem.* **1994**, *33*, 4850.
(131) Allen, F. H.; Davies, J. E.; Galloy, J. J.; Johnson, O.; Kennard, O.; Macrae, C. F.; Mitchell, E. M.; Mitchell, G. F.; Smith, J. M.; Watson, D. G. *J. Chem. Inf. Comput. Sci.* **1991**, *31*, 187.
(132) Vedani, A.; Huhta, D. W. *J. Am. Chem. Soc.* **1990**, *112*, 4759.
(133) Jacober, S. P. SOLVGEN: An Approach to Protein Hydration. M.S. Thesis, Department of Computer Sciences, University of Kansas, 1988.
(134) Cook, C. M.; Allen, L. C. In *Biology and Chemistry of the Carbonic Anhydrases*; Tashian, R. E., Hewett-Emmett, D., Eds. *Ann. New York Acad. Sci.* **1984**, *429*, 84.
(135) Henkens, R. W.; Merril, S. P.; Williams, T. J. In *Biology and Chemistry of the Carbonic Anhydrases*; Tashian, R. E., Hewett-Emmett, D., Eds. *Ann. New York Acad. Sci.* **1984**, *429*, 143.
(136) Menziani, M. C.; De Benedetti, P. G.; Gago, F.; Richards, W. G. *J. Med. Chem.* **1989**, *32*, 951.
(137) Dewar, M. J. S.; Zoebisch, E. G.; Healey, E. F.; Steward, J. J. P. *J. Am. Chem. Soc.* **1985**, *107*, 3902.
(138) Bernstein, F. C.; Koetzle, T. F.; Williams, G. J. B.; Meyer, E. F.; Brice, M. D.; Rodgers, J. R.; Kennard, O.; Shimanouchi, T.; Tasumi, M. *J. Mol. Biol.* **1977**, *122*, 535.
(139) Dewar, M. J. S.; Thiel, W. *J. Am. Chem. Soc.* **1977**, *99*, 4907.
(140) Banci, L.; Bertini, I.; Carloni, P.; Luchinat, C.; Orioli, P. L. *J. Am. Chem. Soc.* **1992**, *114*, 10683.
(141) Manchanda, R.; Zimmer, M.; Brudvig, G.; Crabtree, R. *J. Mol. Struct.* **1994**, *323*, 257.
(142) Scheidt, W. R.; Lee, Y. J. *Struct. Bonding* **1987**, *64*, 1.
(143) Kottalam, J.; Case, D. A. *J. Am. Chem. Soc.* **1988**, *110*, 7690.
(144) Lopez, M., A.; Kollman, P. A. *J. Am. Chem. Soc.* **1989**, *111*, 6212.
(145) Kollman, P. A.; Grootenhuis, P. D. J.; Lopez, M. A. *Pure Appl. Chem.* **1989**, *61*, 593.
(146) (a) Hancock, R. H.; Weaving, J. S.; Marques, H. M. *J. Chem. Soc., Chem. Commun.* **1989**, 1176. (b) Munro, O. Q.; Marques, H. M.; Debrunner, P. G.; Mohanrao, K.; Scheidt, W. R. *J. Am. Chem. Soc.* **1995**, *117*, 935.
(147) Wiberg, K. B.; Boyd, R. H. *J. Am. Chem. Soc.* **1972**, *94*, 8426.
(148) Safo, M.; Walker, F. A.; Raitsimring, A. M.; Walters, W. P.; Dolata, D. P.; Debrunner, P. G.; Scheidt, W. R. *J. Am. Chem. Soc.* **1994**, *116*, 7760.
(149) Abraham, R. J.; Marsden, I. *Tetrahedron* **1992**, *48*, 7489.

(150) Griffiths, L. Ph.D. Thesis, University of Liverpool, 1979.
(151) Abraham, R. J.; Grant, G. H.; Haworth, I. S.; Smith, P. E. *J. Comput. Aided Mol. Des.* **1991**, *5*, 21.
(152) Ostovic, D.; Bruice, T. *J. Am. Chem. Soc.* **1988**, *110*, 6906.
(153) Karaman, R.; Bruice, T. C. *J. Org. Chem.* **1991**, *56*, 3470.
(154) Dauber-Osguthorpe, P.; Roberts, V. A.; Osguthorpe, D. J.; Wolff, J.; Genest, M.; Hagler, A. T. *Proteins: Struct., Funct., Genet.* **1988**, *4*, 31.
(155) Angelucci, L.; De Gioia, L.; Fantucci, P. *Gazz. Chim. Ital.* **1993**, *123*, 111.
(156) Suh, M. P.; Swepston, P. N.; Ibers, J. A. *J. Am. Chem. Soc.* **1984**, *106*, 5164.
(157) Kaplan, W. A.; Scott, R. A.; Suslick, K. S. *J. Am. Chem. Soc.* **1990**, *112*, 1283.
(158) Allinger, N. L.; Flanagan, H. L. *J. Comput. Chem.* **1983**, *4*, 399.
(159) Liljefors, T.; Tai, J. C.; Li, S.; Allinger, N. L. *J. Comput. Chem.* **1987**, *8*, 1051.
(160) Kaplan, W. A.; Scott, R. A.; Suslick, K. S. *J. Am. Chem. Soc.* **1991**, *113*, 9824.
(161) Hancock, R. D.; Dobson, S. M.; Evers, A.; Wade, P.; Ngwenya, M. P.; Boeyens, J. C. A.; Wainwright, K. P. *J. Am. Chem. Soc.* **1988**, *110*, 2788.
(162) McDougall, G. J.; Hancock, R. D.; Boeyens, J. C. A. *J. Chem. Soc., Dalton Trans.* **1978**, 1438.
(163) Zimmer, M. *J. Biomol. Struct. Dyn.* **1993**, *11*, 203.
(164) Collins, J. R.; Camper, D. L.; Loew, G. H. *J. Am. Chem. Soc.* **1991**, *113*, 2736.
(165) Ortiz de Montellano, P. R.; Fruetel, J. A.; Collins, J. R.; Camper, D. L.; Loew, G. H. *J. Am. Chem. Soc.* **1991**, *113*, 3195.
(166) Fruetel, J. A.; Collins, J. R.; Camper, D. L.; Loew, G. H.; Ortiz de Montellano, P. R. *J. Am. Chem. Soc.* **1992**, *114*, 6987.
(167) Fruetel, J. A.; Chang, Y.-T.; Collins, J. R.; Loew, G. H.; Ortiz de Montellano, P. R. *J. Am. Chem. Soc.* **1994**, *116*, 11643.
(168) Harris, D. L.; Loew, G. H. *J. Am. Chem. Soc.* **1994**, *116*, 11671.
(169) Abe, M.; Kitagawa, T.; Kyogoku, Y. *J. Chem. Phys.* **1978**, *69*, 4526.
(170) Li, X.-Y.; Czernuszewicz, R. S.; Kincaid, J. R.; Spiro, T. G. *J. Am. Chem. Soc.* **1989**, *111*, 7012.
(171) Li, X.-Y.; Czernuszewicz, R. S.; Kincaid, J. R.; Stein, P.; Spiro, T. G. *J. Phys. Chem.* **1990**, *94*, 47.
(172) Brennan, T. D.; Scheidt, W. R.; Shelnutt, J. A. *J. Am. Chem. Soc.* **1988**, *110*, 3919.
(173) Medforth, C. J.; Senge, M. O.; Smith, K. M.; Sparks, L. D.; Shelnutt, J. A. *J. Am. Chem. Soc.* **1992**, *114*, 9859.
(174) Anderson, K. K.; Hobbs, J. D.; Luo, L.; Stanley, K. D.; Quirke, J. M. E.; Shelnut, J. A. *J. Am. Chem. Soc.* **1993**, *115*, 12346.
(175) Medforth, C. J.; Berber, M. D.; Smith, K. M.; Shelnutt, J. A. *Tetrahedron Lett.* **1990**, *31*, 3719.
(176) Senge, M. O.; Medforth, C. J.; Sparks, L. D.; Shelnutt, J. A.; Smith, K. M. *Inorg. Chem.* **1993**, *32*, 1716.
(177) Sparks, L. D.; Anderson, K. K.; Medforth, C. J.; Smith, K. M.; Shelnutt, J. A. *Inorg. Chem.* **1994**, *33*, 2297.
(178) Hobbs, J. D.; Majumder, S. A.; Luo, L.; Sickelsmith, G. A.; Quirke, J. M. E.; Medforth, C. J.; Smith, K. M.; Shelnutt, J. A. *J. Am. Chem. Soc.* **1994**, *116*, 3261.
(179) Maruyama, K.; Nagata, T.; Osuka, A. *J. Phys. Org. Chem.* **1988**, *1*, 63.
(180) Cheng, B.; Hobbs, J. D.; Debrunner, P. G.; Erlebacher, J.; Shelnutt, J. A.; Scheidt, W. R. *Inorg. Chem.* **1995**, *34*, 102.
(181) Wojaczynski, J.; Latos-Grazynski, L. *Inorg. Chem.* **1995**, *34*, 1044.
(182) Wojaczynski, J.; Latos-Grazynski, L. *Inorg. Chem.* **1995**, *34*, 1054.
(183) Stratemeier, H.; Hitchman, M. A.; Comba, P.; Bernhardt, P. V.; Riley, M. J. *Inorg. Chem.* **1991**, *30*, 4088.
(184) Comba, P. *Inorg. Chem.* **1994**, *33*, 4577.
(185) Bernhardt, P. V.; Comba, P. *Inorg. Chem.* **1993**, *32*, 2798.
(186) Volbeda, A.; Charon, M.-H.; Piras, C.; Hatchikian, E. C.; Frey, M.; Fontecilla-Camps, J. C. *Nature* **1995**, *373*, 580.
(187) Kim, J.; Rees, D. C. *Science* **1992**, *257*, 1677.
(188) Kim, J.; Rees, D. C. *Nature* **1992**, *360*, 553.

CR9400525